



Localization effects in micropolar laminated composites with imperfect contact conditions

Raffaella Rizzoni ^a, Michele Serpilli ^b, Reinaldo Rodríguez-Ramos ^{c,d},
Yoanh Espinosa-Almeyda ^e, Frédéric Lebon ^f, Maria Letizia Raffa ^g, Serge Dumont ^h

^a Department of Engineering, University of Ferrara, Ferrara, Italy

^b Department of Civil and Building Engineering, and Architecture, Università Politecnica delle Marche, Ancona, Italy

^c Facultad de Matemática y Computación, Universidad de La Habana, San Lázaro y L, Vedado, La Habana, Cuba

^d PPG-MCCT, Universidade Federal Fluminense, Rio de Janeiro, Brazil

^e Instituto de Ingeniería y Tecnología, Universidad Autónoma de Ciudad Juárez, Ciudad Juárez, Chihuahua, Mexico

^f Aix Marseille University, CNRS, Centrale Marseille, LMA, Marseille, France

^g Laboratoire QUARTZ, EA 7393, ISAE-Supméca, Saint-Ouen-sur-Seine, France

^h Laboratoire LAMPS, Université de Perpignan France, 66860 Perpignan, France

ARTICLE INFO

Keywords:

Micropolar elasticity
Laminate
Homogenization
Strain concentration
Stress concentration

ABSTRACT

Within the framework of three-dimensional linear micropolar media, the Asymptotic Homogenization Method (AHM) has been recently applied to obtain the effective engineering moduli for a laminated composite with imperfect contact between the layers. The imperfect contact is prescribed by using a micropolar spring-type interface model, and the interface parameters enter the engineering constants related to the stiffness and torque. In this work, we obtain the concentration tensors linking the macroscopic averaged quantities (stress/couple-stress and strain/curvature) with their microscopic counterparts. A numerical example is proposed to illustrate the influence of the phases volume fraction and of the interface parameters on the strain/curvature and stress/couple-stress concentrations.

1. Introduction

In the last decades, composite materials and structures gained large popularity due to their integration into mechanical and civil engineering, aerospace, automotive, and marine applications, as well as in biomedical and sports products. The successful use of composites in practical applications significantly depends on the ability to accurately predict their mechanical properties and behavior using suitable mechanical models. Micromechanical modeling of composite structures is often challenging due to the complex distribution and orientation of multiple inclusions and reinforcements within the matrix, along with their local mechanical interactions. Hence, it is essential to develop multi-scale approaches that effectively link the microstructure to the overall behavior whilst based on rigorous mathematical techniques. Homogenization techniques offer a viable route and have been applied in many cases in micromechanics of composites, see for instance [1–9] and references therein. Among homogenization techniques, asymptotic homogenization allows rephrasing an initial equilibrium problem, involving one or more small parameters related to the small scale of

the microstructure, into an equilibrium problem for a homogeneous solid. The effective properties of this homogeneous equivalent material are determined by solving local problems defined on the composite material's unit cell. Notably, asymptotic homogenization enables us to determine with a high accuracy the local stress and strain distributions defined by the microstructure of the composite material. The reconstruction of the local stress field results has a pivotal role in developing strength criteria from homogenized modeling approaches. In the literature, other homogenization approaches allow the representation of the local fields, see, for example, the locally-exact homogenization theory based on the Fourier's series proposed in [10,11], and the equivalent inhomogeneity method proposed in [12,13].

Among composites, laminates are multilayered materials composed of alternating layers of different materials. Layered materials are widely used in many fields, such as aerospace engineering, automotive industries, electromechanical systems, and smart structures. Imperfections at the interfaces between the layers are inevitably introduced through the

* Corresponding author.

E-mail addresses: raffaella.rizzoni@unife.it (R. Rizzoni), m.serpilli@univpm.it (M. Serpilli), rerora2006@gmail.com (R. Rodríguez-Ramos), yoanh.espinosa@uacj.mx (Y. Espinosa-Almeyda), lebon@lma.cnrs-mrs.fr (F. Lebon), maria-letizia.raffa@isae-supmecca.fr (M.L. Raffa), serge.dumont@univ-perp.fr (S. Dumont).

<https://doi.org/10.1016/j.compstruct.2025.118898>

Received 1 July 2024; Received in revised form 11 December 2024; Accepted 23 January 2025

Available online 6 February 2025

0263-8223/© 2025 The Authors. Published by Elsevier Ltd. This is an open access article under the CC BY license (<http://creativecommons.org/licenses/by/4.0/>).

manufacturing processes [14–16]. These defects can lead to debonding or slippage, and ultimately to overall performance degradation. A correct approach should incorporate their presence, and the spring-type interface is a classical modeling choice, owing to its mathematical simplicity [5,17]. The spring-type interface is a contact model prescribing the traction vector field to be continuous at the interface and linked to the jump discontinuity of the displacement vector field by a second-order stiffness tensor, usually diagonal, whose components represent the stiffness of the springs in the tangential and normal directions. Using asymptotic techniques, it can be shown that the spring-type interface is an imperfect contact model arising as the limit behavior of a very thin layer made of a soft elastic material [18–20]. The validity of the spring-type interface model has been experimentally assessed by observations based on laser profilometry [21], or ultrasound analysis [22]. In [23], the spring-type interface model has been proven to correctly reproduce the peeling stress distribution along the adherents/adhesive interfaces calculated using the finite element analysis for a thin adhesive interphase.

Nevertheless, the aforementioned models, conceived within the settings of linear elasticity, are unable to accurately describe the mechanical behavior of materials with microstructure, such as molecules, grains, fibers, or pores, and also size-dependent phenomena, which becomes more and more pronounced as the composite structure reduces its size to the micro/nano-scale. The effect of microstructure and size effects can be adequately modeled with higher-order continuum theories such as micropolar elasticity, see e.g. [11,24–27]. In order to take into account the possible influence of the internal microstructure among the composite constituents, classical elastic contact models have been recently generalized in the framework of micropolar elasticity [28] and strain gradient elasticity [29].

In the literature, numerous studies are devoted to the derivation of the effective elastic properties of layered materials under the presence of imperfect adhesion, cf. [17]. Among these, Brito-Santana et al. have applied the two-scale asymptotic homogenization method to obtain the effective elastic properties of laminates characterized by non-uniform imperfect adhesion [30] and by localized damage in the interface between the layers [31]. Recently, Fergoug et al. [32] have proposed an approach based on asymptotic homogenization to estimate consistent microscale fields in the vicinity of the boundaries. Notably, classical laminate theory successfully applies to obtaining the effective response of laminates in form of plate-like solids, for which the thickness is much smaller than the other characteristic dimensions [33,34]. Here, the object of the investigation is not a plate-like solid but a laminate intended as a stratified material, cf. [6,35].

A possible application of the present analysis could, for example, find application in the Earth's sciences, where micropolar theory has been shown to better described the effect of rotational motions during seismogenic deformation compared to the linear elastic theory, cf. [36] and references therein. Micropolar theory has recently found interesting applications in the description of lattice metamaterials, see for example [37]. Recent advances in modern nanotechnology open to the fabrication of periodic stratified metamaterials to tune the transmissivity within the frequency band of negative refraction [38].

The present study stems from some recent work, where the homogenized properties of a stratified material composed of alternating micropolar thin layers under imperfect contact conditions have been obtained using the two-scale asymptotic homogenization method [39–41]. The motivation of the present work is the reconstruction of the local stress field from the homogenization results, a field that could possibly enter a homogenized strength criterion of the type proposed in [42]. Our work represents a proposal for the development of tools in the framework of homogenization theory useful for the computation of the local stresses. The evaluation of the latter ones is crucial in the assessment of the structural integrity of mechanical components.

After reviewing the main results obtained in [39–41], we evaluate the micropolar strain/curvature and stress/couple-stress concentration

tensors arising from the local strain and stress field. These tensors enable to calculate of the (constant) strain/curvature and stress/couple-stress in the adherent layers given the externally applied (or averaged) strain and stress field. For the type of composite here studied, a stratified medium composed of alternated layers of micropolar materials in imperfect contact, the calculation of the stress and strain concentration tensors in the layers together with the displacement and microrotation jump concentration tensors at the imperfect interface are all elements of novelty. The effect of imperfection parameters of the interface on the concentration tensors is investigated. Another original result of the present work is that, while strain and curvature concentration tensors are found to depend on the interface parameters, the stress and couple-stress concentration tensors are not. This outcome is not a foregone conclusion. To better understand and validate this result, a simple example is proposed in the framework of linear elasticity, indicating that the independence of the stress and couple stress in the adherent layers may be attributed to the simple nature of the interface law chosen to model the imperfect contact. Finally, a numerical application is presented to study the effect of a uniform imperfect interface on the local values of strain and stress in a bi-laminated composite with centro-symmetric micropolar isotropic constituents.

2. A micropolar laminated elastic continuum with imperfect contact between the layers

Let us consider a linear elastic micropolar continuum in the three-dimensional Euclidean physical space, occupying the reference configuration Ω . Introduced a Cartesian coordinate system $\{O; x_1, x_2, x_3\}$, we assume Ω to be described by a parallelepiped of dimensions L_i ($i = 1, 2, 3$) generated by repetitions of a periodic cell Y along the x_3 -axis. At the microscale, the cell Y is a bi-laminated composite, see Fig. 1, with two constituent material phases denoted as S_γ ($\gamma = 1, 2$) such as $Y = S_1 \cup S_2$, $S_1 \cap S_2 = \emptyset$. Each layer S_γ is characterized by the volume fraction V_γ , with $V_1 + V_2 = 1$, and l_i is the cell length in the y_i -direction. Imperfect contact conditions are assumed at the interface region Γ between the layers, following contact laws to be specified later.

At the macroscale, two independent fields, the displacement $u_i(\mathbf{x})$ and the microrotation $\omega_i(\mathbf{x})$, characterize the degrees of freedom of the continuum at each material point \mathbf{x} , cf. [26].

In the case of small displacements, microrotations, deformations and curvatures, at equilibrium the linear and angular balance equations must hold

$$\sigma_{ji,j}(\mathbf{x}) + f_i(\mathbf{x}) = 0, \quad \mu_{ji,j}(\mathbf{x}) + \epsilon_{ijk}\sigma_{jk}(\mathbf{x}) + g_i(\mathbf{x}) = 0, \quad \text{in } S_1 \cup S_2, \quad (1)$$

where $\sigma_{ji}(\mathbf{x})$ [N/m²] is the (non-symmetric) stress tensor, $\mu_{ji}(\mathbf{x})$ [N/m] is the couple-stress tensor, $f_i(\mathbf{x})$ [N/m³] are the body forces, $g_i(\mathbf{x})$ [N/m²] are the body couples functions, ϵ_{ijk} is the Levi-Civita's alternator tensor and a comma indicates partial derivative. Einstein's summation convention is used Latin indices take values in the set $\{1, 2, 3\}$, while Greek indices are in the set $\{1, 2\}$, cf. also [39–41] for the index notation. Note also that the addition of the extra microrotation field variables, $\omega_i(\mathbf{x})$, removes the symmetry of the Cauchy stress tensor, a condition that is replaced by the second set of equations in (1).

The model of linear micropolar centro-symmetric continuum is based on the following two constitutive relations

$$\sigma_{ji}(\mathbf{x}) = C_{ijmn}(\mathbf{x}) e_{nm}, \quad \mu_{ji}(\mathbf{x}) = D_{ijmn}(\mathbf{x}) \psi_{nm} \quad \text{in } S_1 \cup S_2, \quad (2)$$

linking the stresses, $\sigma_{ji}(\mathbf{x})$ and $\mu_{ji}(\mathbf{x})$, with the micropolar strain $e_{mn}(\mathbf{x})$ and the torsion-curvature $\psi_{mn}(\mathbf{x})$ [m⁻¹] tensors, respectively, defined as

$$e_{nm}(\mathbf{x}) = u_{m,n}(\mathbf{x}) + \epsilon_{mns}\omega_s(\mathbf{x}), \quad \psi_{nm}(\mathbf{x}) = \omega_{m,n}(\mathbf{x}) \quad \text{in } S_1 \cup S_2. \quad (3)$$

In Eqs. (2) and (3), the symmetric part of $e_{mn}(\mathbf{x})$ corresponds to the classical strain tensor whereas its skew-symmetric part accounts for the local reorientation of the microstructure. In the context of linear micropolar elasticity as proposed by Eringen, for the free energy density

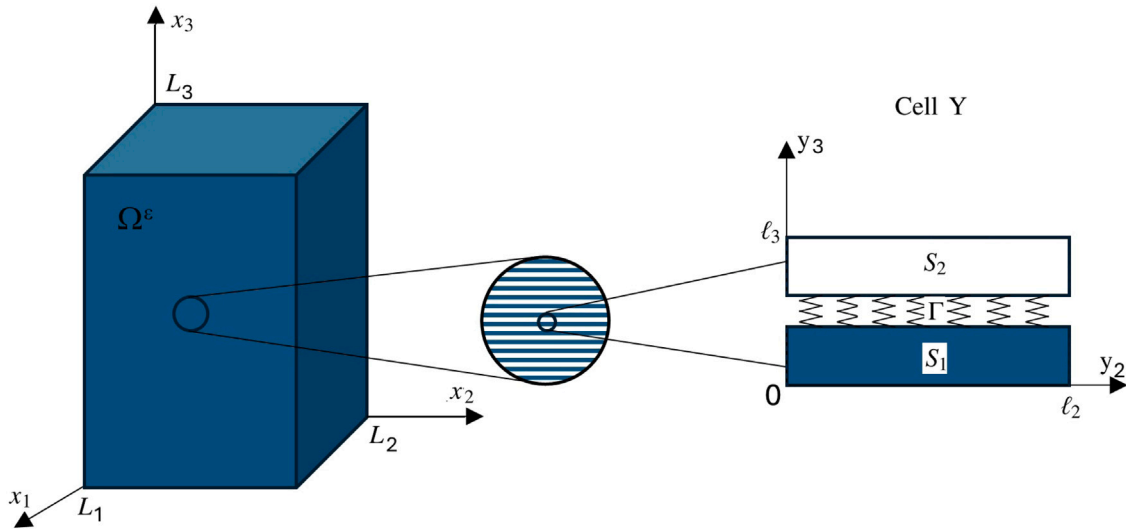


Fig. 1. Laminated micropolar composite with the detail of the unit cell Y composed of two different laminae in contact through a layer of linear springs.

to be invariant, the term coupling e_{nm} and ψ_{nm} in the constitutive equations must vanish, see discussion after Eqn. (20.10) in [26]. Also, the major symmetry conditions $C_{ijmn}(\mathbf{x}) = C_{mnij}(\mathbf{x})$ and $D_{ijmn}(\mathbf{x}) = D_{mnij}(\mathbf{x})$ are satisfied, cf. [26, Eqns. (20.11)].

The equilibrium problem of the micropolar continuum is described by the system of Eqs. (1)–(3) together with the boundary conditions on $\partial\Omega$. The boundary $\partial\Omega$ is assumed to be made of four regular disjoint surfaces, $\partial\Omega_i, i = 1, 2, 3, 4$, such that $\partial\Omega = \bigcup_{i=1}^4 \partial\Omega_i$, and on which the displacements, microrotations, surface forces, and surface couples are assigned. In particular, the domain Ω is constrained in such a way that the displacements u_i vanish on $\partial\Omega_1$, the microrotations ω_i vanish on $\partial\Omega_2$, the tractions $\sigma_{ji}n_j$ are assigned on $\partial\Omega_3$, and the moments $\mu_{ji}n_j$ are assigned on $\partial\Omega_4$, as follows:

$$\begin{aligned} u_i(\mathbf{x})|_{\partial\Omega_1} &= 0, & (C_{ijmn}(\mathbf{x})e_{nm}(\mathbf{x}))n_j|_{\partial\Omega_2} &= F_i(\mathbf{x}), \\ \omega_i(\mathbf{x})|_{\partial\Omega_2} &= 0, & (D_{ijmn}(\mathbf{x})\psi_{nm}(\mathbf{x}))n_j|_{\partial\Omega_4} &= G_i(\mathbf{x}), \end{aligned} \quad (4)$$

where $F_i(\mathbf{x})$ and $G_i(\mathbf{x})$ are the surface forces and moments. The formulation defined by Eqs. (1)–(4) represents the static boundary value problem associated with the linear theory of micropolar elasticity whose coefficients are rapidly oscillating. Also, in Eq. (4), n_j denotes the unit outer normal vector to $\partial\Omega$.

In addition to Eqs. (1)–(4), contact conditions at the interface Γ between the laminae S_1, S_2 of the cells are prescribed, following the spring model:

$$\begin{aligned} (C_{ijmn}(\mathbf{x})e_{nm}(\mathbf{x}))n_j &= K_{ij} \llbracket u_j \rrbracket, & \llbracket (C_{ijmn}(\mathbf{x})e_{nm}(\mathbf{x}))n_j \rrbracket &= 0 \text{ on } \Gamma, \\ (D_{ijmn}(\mathbf{x})\psi_{nm}(\mathbf{x}))n_j &= Q_{ij} \llbracket \omega_j \rrbracket, & \llbracket (D_{ijmn}(\mathbf{x})\psi_{nm}(\mathbf{x}))n_j \rrbracket &= 0 \text{ on } \Gamma, \end{aligned} \quad (5)$$

where $\llbracket p \rrbracket = p^{(1)} - p^{(2)}$ is taken to denote the jump of the function p across the interface Γ . The symbols K_{ij} [N/m³] and Q_{ij} [N/m] are

the interface material parameters, such that $(K_{ij}) = \begin{pmatrix} K_1 & 0 & 0 \\ 0 & K_2 & 0 \\ 0 & 0 & K_3 \end{pmatrix}$

and $(Q_{ij}) = \begin{pmatrix} Q_1 & 0 & 0 \\ 0 & Q_2 & 0 \\ 0 & 0 & Q_3 \end{pmatrix}$. Here, K_1, K_2, Q_1 , and Q_2 are the interface parameters in the tangential directions, while K_3 and Q_3 are the interface parameters in the normal direction of the interface Γ .

The coefficients K_i have a clear physical meaning, directly related to the material (type of material symmetry, elastic constants) and geometrical (thickness) parameters of the adhesive. For example, for an isotropic adhesive material, the tangential stiffness components K_1, K_2 are equal to μ/h and the normal stiffness component K_3 is given by $(2\mu + \lambda)/h$, where λ, μ are the Lamé's moduli of the adhesive and

h is its thickness [20,43,44]. An equivalent form of the imperfect contact conditions (5), together with a clear physical interpretation of the coefficients Q_i , have been rigorously obtained for soft micropolar interfaces by applying asymptotic techniques in [28].

3. Summary of results of asymptotic homogenization method and effective engineering moduli for periodic laminated micropolar media

In this framework, the applied methodology based on the AHM for centro-symmetric micropolar laminate composites with perfect contact conditions [39,41] is implemented in the case of an uniform imperfect interface. The AHM provides averaged expressions for the rapidly oscillating elasticity tensors of the original problem and proposes a homogeneous equivalent medium with the same behavior. Its main assumptions are that all fields are considered as power series of the small and positive definite dimensionless parameter ε whose coefficients are dependent on the macro (\mathbf{x}) and micro (\mathbf{y}) scales, see, for instance, [3,4,9,45]. Both scales are related as $\mathbf{y} = \mathbf{x}/\varepsilon$, where $\varepsilon = \ell/L \ll 1$ is defined by the ratio between the characteristic size of the periodicity cell (ℓ) and the diameter of the body (L).

The AHM starts from the substitution of the expansions for the displacements $u_m^\varepsilon(\mathbf{x})$ and the microrotations $\omega_m^\varepsilon(\mathbf{x})$

$$u_m^\varepsilon(\mathbf{x}) = \sum_{\alpha=0}^{\infty} \varepsilon^\alpha u_m^{(\alpha)}(\mathbf{x}, \mathbf{y}), \quad \omega_m^\varepsilon(\mathbf{x}) = \sum_{\alpha=0}^{\infty} \varepsilon^\alpha \omega_m^{(\alpha)}(\mathbf{x}, \mathbf{y}), \quad (6)$$

into the problem (Eqs. (1)–(5)), and following algebraic operations and differentiation rules. Here, $u_m^{(i)}(\mathbf{x}, \mathbf{y})$ and $\omega_m^{(i)}(\mathbf{x}, \mathbf{y})$ ($i = 0, 1, 2, \dots$) are infinitely differentiable and Y -periodic functions with respect to \mathbf{y} . Thus, a sequence of problems given by partial differential equations is obtained in relation to the power of the ε parameter. From them, the formulation of local problems on Y , the effective moduli, and the equivalent homogenized problem with its asymptotic solution is obtained. Details about the AHM methodology related to micropolar laminated composites are shown in [39,41] and are summarized in the sequel.

The order zero terms of the asymptotic expansion (Eq. (6)), namely $u_m^{(0)}$ and $\omega_m^{(0)}$, are proved to be independent of the local variable \mathbf{y} , so that $u_m^{(0)}(\mathbf{x}, \mathbf{y}) = u_m^{(0)}(\mathbf{x})$ and $\omega_m^{(0)}(\mathbf{x}, \mathbf{y}) = \omega_m^{(0)}(\mathbf{x})$. Besides, the first order terms $u_m^{(1)}$ and $\omega_m^{(1)}$ can be expressed as follows:

$$u_m^{(1)}(\mathbf{x}, \mathbf{y}) = \rho_q N_m \left(u_{p,q}^{(0)} + \varepsilon_{pq5} \omega_s^{(0)} \right) + \tilde{u}_m^{(1)}, \quad \omega_m^{(1)}(\mathbf{x}, \mathbf{y}) = \rho_q M_m \omega_{p,q}^{(0)} + \tilde{\omega}_m^{(1)}, \quad (7)$$

where ${}_{pq}N_m$ and ${}_{pq}M_m$ are the local pq -displacements and pq -microrotations defined in the cell Y , respectively. The terms $\bar{u}_m^{(1)}$ and $\bar{\omega}_m^{(1)}$ are constant functions. Functions ${}_{pq}N_m$ and ${}_{pq}M_m$ only depend on y_3 and satisfy the periodicity conditions ${}_{pq}N_m(0) = {}_{pq}N_m(\ell_i)$ and ${}_{pq}M_m(0) = {}_{pq}M_m(\ell_i)$.

The local functions ${}_{pq}N_m$ and ${}_{pq}M_m$ can be explicitly characterized as shown in [39,41] and they verify:

$${}_{pq}N'_m = C_{m3i3}^{-1} (\alpha_{ipq} - C_{i3pq}), \quad {}_{pq}M'_m = D_{m3i3}^{-1} (\beta_{ipq} - D_{i3pq}), \quad (8)$$

with

$$\begin{aligned} \alpha_{ipq} &= (\langle C_{i3i3}^{-1} \rangle + \ell_3^{-1} K_i^{-1})^{-1} \langle C_{i3c3}^{-1} C_{b3pq} \rangle, \\ \beta_{ipq} &= (\langle D_{i3i3}^{-1} \rangle + \ell_3^{-1} Q_i^{-1})^{-1} \langle D_{i3c3}^{-1} D_{b3pq} \rangle, \end{aligned} \quad (9)$$

where $(\bullet)' = d(\bullet)/dy_3$ and the symbol $\langle p \rangle$ denotes the Voigt's average of the property p , i.e., $\langle p \rangle = \sum_{i=1}^N p^{(i)} V_i$ with N the number of phases in Y and $\sum_{i=1}^N V_i = 1$. In case of a bi-laminated composite, $\langle p \rangle = p^{(1)} V_1 + p^{(2)} V_2$ where $V_1 = c/\ell_3$ and $V_2 = 1 - c/\ell_3$ are the volume fractions per unit length occupied by the layer 1 and 2, respectively; such as, $V_1 + V_2 = 1$. c represents the thickness of the adhesive contact region and ℓ_3 is the cell length in the thickness direction y_3 , related to the small parameter ϵ . The consideration $\ell_3 \rightarrow \infty$ enables us to derive the equivalent expression for a micropolar laminated medium with perfect contact (classical case), where imperfections are absent. However, the existence of imperfections is crucial for analyzing localization effects in this study. Notably, the Voigt's average entering (9) is a result of the asymptotic analysis.

The above relations will help to find effective properties of the laminated composite, which are defined as follows:

$$\begin{aligned} C_{ijpq}^* &= \langle C_{ijpq} + C_{ijm3} {}_{pq}N'_m \rangle, \\ D_{ijpq}^* &= \langle D_{ijpq} + D_{ijm3} {}_{pq}M'_m \rangle. \end{aligned} \quad (10)$$

By replacing the expression Eq. (8) into Eq. (10), the corresponding stiffness and torque effective properties are obtained as functions of the constituent properties, the imperfection parameters and the constituent volume fraction, see for instance, Rodríguez-Ramos et al. [39]:

$$\begin{aligned} C_{ijpq}^* &= \langle C_{ijpq} - C_{ijm3} C_{m3a3}^{-1} C_{a3pq} \rangle + \langle C_{ijm3} C_{m3a3}^{-1} \rangle (\langle C_{a3a3}^{-1} \rangle \\ &\quad + \ell_3^{-1} K_a^{-1})^{-1} \langle C_{a3c3}^{-1} C_{c3pq} \rangle, \\ D_{ijpq}^* &= \langle D_{ijpq} - D_{ijm3} D_{m3a3}^{-1} D_{a3pq} \rangle + \langle D_{ijm3} D_{m3a3}^{-1} \rangle (\langle D_{a3a3}^{-1} \rangle \\ &\quad + \ell_3^{-1} Q_a^{-1})^{-1} \langle D_{a3c3}^{-1} D_{c3pq} \rangle. \end{aligned} \quad (11)$$

Let us consider the case of micropolar centro-symmetric isotropic elastic materials, whose elasticity constitutive tensors are defined as follows:

$$\begin{aligned} C_{ijmn}^\gamma &= \lambda^\gamma \delta_{ij} \delta_{mn} + (\mu^\gamma + \alpha^\gamma) \delta_{im} \delta_{jn} + (\mu^\gamma - \alpha^\gamma) \delta_{in} \delta_{jm}, \\ D_{ijmn}^\gamma &= \beta^\gamma \delta_{ij} \delta_{mn} + (\kappa^\gamma + \epsilon^\gamma) \delta_{im} \delta_{jn} + (\kappa^\gamma - \epsilon^\gamma) \delta_{in} \delta_{jm}, \end{aligned} \quad (12)$$

where δ_{ij} is the Kronecker's delta tensor and $\lambda^\gamma, \mu^\gamma, \alpha^\gamma, \beta^\gamma, \kappa^\gamma$ and ϵ^γ denote the micropolar elastic constants for the materials in the domains S_γ , with $\gamma = 1, 2$. Among the twelve elastic constants appearing in Eq. (12), λ^γ and μ^γ are the classical Lamé coefficients, with μ^γ the shear moduli of the two layers' materials. The other eight constants, i.e. $\alpha^\gamma, \beta^\gamma, \epsilon^\gamma$ and κ^γ , are the micropolar elastic constants. The classical theory of elasticity is recovered for vanishing micropolar elastic constants.

Substituting the expressions of Eq. (12) into Eq. (11), the 9×9 -matrix of (C_{ijpq}^*) in Voigt's notation takes the form

$$(C_{ijpq}^*) = \begin{pmatrix} C_{1111}^* & C_{1122}^* & C_{1133}^* & 0 & 0 & 0 & 0 & 0 & 0 \\ C_{2211}^* & C_{2222}^* & C_{2233}^* & 0 & 0 & 0 & 0 & 0 & 0 \\ C_{3311}^* & C_{3322}^* & C_{3333}^* & 0 & 0 & 0 & 0 & 0 & 0 \\ 0 & 0 & 0 & C_{2323}^* & 0 & 0 & C_{2332}^* & 0 & 0 \\ 0 & 0 & 0 & 0 & C_{1313}^* & 0 & 0 & C_{1331}^* & 0 \\ 0 & 0 & 0 & 0 & 0 & C_{1212}^* & 0 & 0 & C_{1221}^* \\ 0 & 0 & 0 & C_{3223}^* & 0 & 0 & C_{3232}^* & 0 & 0 \\ 0 & 0 & 0 & 0 & C_{3113}^* & 0 & 0 & C_{3131}^* & 0 \\ 0 & 0 & 0 & 0 & 0 & C_{2112}^* & 0 & 0 & C_{2121}^* \end{pmatrix}, \quad (13)$$

where

$$\begin{aligned} C_{1111}^* &= C_{2222}^* = \left\langle \frac{4\mu(\lambda + \mu)}{\lambda + 2\mu} \right\rangle + \left\langle \frac{\lambda}{\lambda + 2\mu} \right\rangle^2 \left(\frac{1}{\ell_3} K_3^{-1} + \left\langle \frac{1}{\lambda + 2\mu} \right\rangle \right)^{-1}, \\ C_{3333}^* &= \left(\frac{1}{\ell_3} K_3^{-1} + \left\langle \frac{1}{\lambda + 2\mu} \right\rangle \right)^{-1}, \\ C_{1122}^* &= \left\langle \frac{2\lambda\mu}{\lambda + 2\mu} \right\rangle + \left\langle \frac{\lambda}{\lambda + 2\mu} \right\rangle^2 \left(\frac{1}{\ell_3} K_3^{-1} + \left\langle \frac{1}{\lambda + 2\mu} \right\rangle \right)^{-1}, \\ C_{1133}^* &= C_{2233}^* = C_{3311}^* = C_{3322}^* = \left\langle \frac{\lambda}{\lambda + 2\mu} \right\rangle \left(\frac{1}{\ell_3} K_3^{-1} + \left\langle \frac{1}{\lambda + 2\mu} \right\rangle \right)^{-1}, \\ C_{2323}^* &= \left(\frac{1}{\ell_3} K_2^{-1} + \left\langle \frac{1}{\alpha + \mu} \right\rangle \right)^{-1}, \\ C_{1313}^* &= \left(\frac{1}{\ell_3} K_1^{-1} + \left\langle \frac{1}{\alpha + \mu} \right\rangle \right)^{-1}, \\ C_{1212}^* &= C_{2121}^* = \langle \mu + \alpha \rangle, \\ C_{3232}^* &= \left\langle \frac{4\alpha\mu}{\mu + \alpha} \right\rangle + \left\langle \frac{\mu - \alpha}{\mu + \alpha} \right\rangle^2 \left(\frac{1}{\ell_3} K_2^{-1} + \left\langle \frac{1}{\alpha + \mu} \right\rangle \right)^{-1}, \\ C_{3131}^* &= \left\langle \frac{4\alpha\mu}{\mu + \alpha} \right\rangle + \left\langle \frac{\mu - \alpha}{\mu + \alpha} \right\rangle^2 \left(\frac{1}{\ell_3} K_1^{-1} + \left\langle \frac{1}{\mu + \alpha} \right\rangle \right)^{-1}, \\ C_{2332}^* &= \left\langle \frac{\mu - \alpha}{\mu + \alpha} \right\rangle \left(\frac{1}{\ell_3} K_2^{-1} + \left\langle \frac{1}{\alpha + \mu} \right\rangle \right)^{-1}, \\ C_{1331}^* &= \left\langle \frac{\mu - \alpha}{\mu + \alpha} \right\rangle \left(\frac{1}{\ell_3} K_1^{-1} + \left\langle \frac{1}{\mu + \alpha} \right\rangle \right)^{-1}, \\ C_{1221}^* &= C_{2121}^* = \langle \mu - \alpha \rangle. \end{aligned} \quad (14)$$

The effective elastic tensor (C_{ijpq}^*) is thus characterized by twelve independent constants, ten of which depend on the stiffness properties of the interface K_i . In the purely elastic case, i.e. for vanishing micropolar elastic constants, and for perfect contact between the layer, i.e. for $K_i \rightarrow \infty$, tensor (C_{ijpq}^*) reduces to the 6×6 effective elasticity matrix, whose components have been computed by Backus for a horizontally layered medium in [35, Eqns. (8) and (13)].

By taking the inverse of the effective elastic tensor, the compliance effective tensor (S_{ijpq}^*) can be calculated. The 9×9 compliance matrix has the same structure of the effective elastic tensor, presenting vanishing components in the same positions, and it can be expressed in terms of generalized Young's moduli and Poisson's ratios as follows:

$$(S_{ijpq}^*) = \begin{pmatrix} \frac{1}{E_1^*} & -\frac{\nu_{21}^*}{E_2^*} & -\frac{\nu_{31}^*}{E_3^*} & 0 & 0 & 0 & 0 & 0 & 0 \\ -\frac{\nu_{12}^*}{E_1^*} & \frac{1}{E_2^*} & -\frac{\nu_{32}^*}{E_3^*} & 0 & 0 & 0 & 0 & 0 & 0 \\ -\frac{\nu_{13}^*}{E_1^*} & -\frac{\nu_{23}^*}{E_2^*} & \frac{1}{E_3^*} & 0 & 0 & 0 & 0 & 0 & 0 \\ 0 & 0 & 0 & \frac{1}{G_{23}^*} & 0 & 0 & -\frac{\nu_{74}^*}{G_{32}^*} & 0 & 0 \\ 0 & 0 & 0 & 0 & \frac{1}{G_{13}^*} & 0 & 0 & -\frac{\nu_{85}^*}{G_{31}^*} & 0 \\ 0 & 0 & 0 & 0 & 0 & \frac{1}{G_{12}^*} & 0 & 0 & -\frac{\nu_{96}^*}{G_{21}^*} \\ 0 & 0 & 0 & -\frac{\nu_{47}^*}{G_{23}^*} & 0 & 0 & \frac{1}{G_{32}^*} & 0 & 0 \\ 0 & 0 & 0 & 0 & -\frac{\nu_{58}^*}{G_{13}^*} & 0 & 0 & \frac{1}{G_{31}^*} & 0 \\ 0 & 0 & 0 & 0 & 0 & -\frac{\nu_{69}^*}{G_{12}^*} & 0 & 0 & \frac{1}{G_{21}^*} \end{pmatrix}. \quad (15)$$

The engineering constants are related to the material constants of the adherents and of the interface by the relations

$$\begin{aligned}
 E_1^* &= E_2^* = \langle \mu \rangle \left\langle \frac{\mu(3\lambda + 2\mu)}{\lambda + 2\mu} \right\rangle \left\langle \frac{\mu(\lambda + \mu)}{\lambda + 2\mu} \right\rangle^{-1}, \\
 E_3^* &= \left(\frac{1}{\ell_3} K_3^{-1} + \left\langle \frac{1}{\lambda + 2\mu} \right\rangle + \left\langle \frac{\lambda}{\lambda + 2\mu} \right\rangle^2 \left\langle \frac{\mu(3\lambda + 2\mu)}{\lambda + 2\mu} \right\rangle^{-1} \right)^{-1}, \\
 \nu_{12}^* &= \frac{1}{2} \left\langle \frac{\lambda\mu}{\lambda + 2\mu} \right\rangle \left\langle \frac{\mu(\lambda + \mu)}{\lambda + 2\mu} \right\rangle^{-1}, \\
 \nu_{13}^* &= \nu_{23}^* = \frac{1}{2} \left\langle \frac{\lambda}{\lambda + 2\mu} \right\rangle \left\langle \frac{\mu(\lambda + \mu)}{\lambda + 2\mu} \right\rangle^{-1}, \\
 G_{23}^* &= \left(\frac{1}{\ell_3} K_2^{-1} + \left\langle \frac{1}{\mu + \alpha} \right\rangle + \left\langle \frac{\mu - \alpha}{\mu + \alpha} \right\rangle^2 \left\langle \frac{4\mu\alpha}{\mu + \alpha} \right\rangle^{-1} \right)^{-1}, \\
 G_{13}^* &= \left(\frac{1}{\ell_3} K_1^{-1} + \left\langle \frac{1}{\mu + \alpha} \right\rangle + \left\langle \frac{\mu - \alpha}{\mu + \alpha} \right\rangle^2 \left\langle \frac{4\mu\alpha}{\mu + \alpha} \right\rangle^{-1} \right)^{-1}, \\
 G_{12}^* &= G_{21}^* = \left(\frac{1}{4\langle \mu \rangle} + \frac{1}{4\langle \alpha \rangle} \right)^{-1}, \\
 G_{32}^* &= G_{31}^* = \left\langle \frac{4\mu\alpha}{\mu + \alpha} \right\rangle, \\
 \nu_{74}^* &= \nu_{85}^* = \left\langle \frac{\mu - \alpha}{\mu + \alpha} \right\rangle, \\
 \nu_{96}^* &= \nu_{69}^* = \frac{\langle \mu \rangle - \langle \alpha \rangle}{\langle \mu \rangle + \langle \alpha \rangle}.
 \end{aligned} \tag{16}$$

The remaining Poisson's ratios can be calculated using the relations $\nu_{ij}^*/E_i^* = \nu_{ji}^*/E_j^*$, $i, j = 1, 2, 3$, $\nu_{47}^*/G_{23}^* = \nu_{74}^*/G_{32}^*$, and $\nu_{58}^*/G_{13}^* = \nu_{85}^*/G_{31}^*$, that guarantee the symmetry of the compliance matrix. Finally, one finds that $\nu_{47}^*/G_{23}^* = \nu_{58}^*/G_{13}^*$, and $\nu_{74}^*/G_{32}^* = \nu_{85}^*/G_{31}^*$. Notably, the homogenized laminate composite is characterized by ten linearly independent engineering constants, that can be chosen to be E_1^* , E_3^* , G_{23}^* , G_{13}^* , G_{12}^* , G_{32}^* , ν_{12}^* , ν_{13}^* , ν_{74}^* , and ν_{96}^* . Only three of them depend on the elastic properties of the interface: E_3^* , G_{23}^* , and G_{13}^* , which depends on K_3 , K_2 , and K_1 , respectively. The Poisson's ratios ν_{13}^* , ν_{47}^* , and ν_{58}^* also depend on K_3 , K_2 , and K_1 , respectively.

As seen above, the effective elastic tensor (C_{ijpq}^*) was characterized by twelve elastic constants, while its inverse (S_{ijpq}^*) turned out to be characterized by ten elastic coefficients, two less. This is due to the fact that, if $K_1 \neq K_2$, the components C_{3232}^* and C_{3131}^* are different from each other, as the components C_{2332}^* and C_{1331}^* . In contrast, one can find that $G_{32}^* = G_{31}^*$, implying $S_{3232}^* = S_{3131}^*$, and $\nu_{74}^*/G_{32}^* = \nu_{85}^*/G_{31}^*$, implying $S_{2332}^* = S_{1331}^*$.

Since both the effective tensors (C_{ijpq}^*) and (D_{ijpq}^*) in Eqs. (11) have the same structure, only the analytical expressions for the (C_{ijpq}^*) and its inverse have been shown. The analytical expressions of the components of (D_{ijpq}^*), of its inverse (\tilde{S}_{ijpq}^*) and of the effective engineering moduli related to torque, \tilde{E}_1^* , \tilde{E}_3^* , ..., can be found by replacing λ, μ and α , with β, κ and ϵ , respectively.

A numerical example illustrating the variation of the effective engineering moduli with the volume fraction of the adherents and the imperfection parameters has been given in [40].

4. Micropolar strain/curvature and stress/couple-stress concentration tensors

Following the approach proposed in [3] for heterogeneous elastic materials, local microscopic quantities, such as strains and stresses, curvatures, and couple stresses, can be connected with their macroscopic counterparts via relations of the form:

$$\begin{aligned}
 e_{ji}(\mathbf{x}, \mathbf{y}) &= A_{ijpq}(\mathbf{y}) \bar{e}_{qp}(\mathbf{x}), & \sigma_{ji}(\mathbf{x}, \mathbf{y}) &= B_{ijpq}(\mathbf{y}) \bar{\sigma}_{qp}(\mathbf{x}), \\
 \psi_{ji}(\mathbf{x}, \mathbf{y}) &= \tilde{A}_{ijpq}(\mathbf{y}) \bar{\psi}_{qp}(\mathbf{x}), & \mu_{ji}(\mathbf{x}, \mathbf{y}) &= \tilde{B}_{ijpq}(\mathbf{y}) \bar{\mu}_{qp}(\mathbf{x}),
 \end{aligned} \tag{17}$$

with \bar{e}_{qp} , $\bar{\sigma}_{qp}$, $\bar{\psi}_{qp}$ and $\bar{\mu}_{qp}$ denote the average strain, stress, curvature, and couple stress, respectively (see e.g. [2]). In these expressions, A_{ijpq} , B_{ijpq} , \tilde{A}_{ijpq} and \tilde{B}_{ijpq} represent the strain concentration tensor, the stress concentration tensor, the microcurvature concentration, and

the couple-stress concentration tensor, respectively. In periodic asymptotic homogenization, the strain concentration tensor arising from the displacement field over the cell Y is given by

$$A_{ijpq} := I_{ijpq} + {}_{pq}N_{i|j}, \quad \tilde{A}_{ijpq} := I_{ijpq} + {}_{pq}M_{i|j}, \tag{18}$$

where $I_{ijpq} := \delta_{ip}\delta_{jq}$ is the fourth-order identity tensor, and ${}_{pq}N_{i|j}$ and ${}_{pq}M_{i|j}$ represent the derivatives with respect to the local coordinate y_j of the local problem solutions. As shown in the previous Section 4, for laminates whose layered direction is along the y_3 -axis, the solutions ${}_{pq}N_j$ and ${}_{pq}M_j$ depend only on the local variable y_3 . Thus, the components of A_{ijpq} simplifies as

$$A_{i\beta pq}^\gamma = I_{i\beta pq}, \quad A_{\alpha 3 pq}^\gamma = I_{\alpha 3 pq} + ({}_{pq}N_\alpha^\gamma)', \quad A_{33 pq}^\gamma = I_{33 pq} + ({}_{pq}N_3^\gamma)', \tag{19}$$

where the superscript $\gamma = 1, 2$ indicates the layers of the periodic bilaminated composite, and, thus, the top and bottom adherents within the cell Y , respectively. Clearly, the same properties hold for tensor $\tilde{A}_{i\beta pq}^\gamma$.

In view of Eqs. (8) and (12), the strain concentration tensor takes the following form:

$$(A_{ijpq}^\gamma) = \begin{pmatrix} 1 & 0 & 0 & 0 & 0 & 0 & 0 & 0 & 0 \\ 0 & 1 & 0 & 0 & 0 & 0 & 0 & 0 & 0 \\ A_{3311}^\gamma & A_{3322}^\gamma & A_{3333}^\gamma & 0 & 0 & 0 & 0 & 0 & 0 \\ 0 & 0 & 0 & A_{2323}^\gamma & 0 & 0 & A_{2332}^\gamma & 0 & 0 \\ 0 & 0 & 0 & 0 & A_{1313}^\gamma & 0 & 0 & A_{1331}^\gamma & 0 \\ 0 & 0 & 0 & 0 & 0 & 1 & 0 & 0 & 0 \\ 0 & 0 & 0 & 0 & 0 & 0 & 1 & 0 & 0 \\ 0 & 0 & 0 & 0 & 0 & 0 & 0 & 1 & 0 \\ 0 & 0 & 0 & 0 & 0 & 0 & 0 & 0 & 1 \end{pmatrix}, \tag{20}$$

with

$$\begin{aligned}
 A_{3311}^\gamma &= A_{3322}^\gamma = \frac{b_3}{\lambda^\gamma + 2\mu^\gamma} \left\langle \frac{\lambda}{\lambda + 2\mu} \right\rangle - \frac{\lambda^\gamma}{\lambda^\gamma + 2\mu^\gamma}, \\
 A_{3333}^\gamma &= \frac{b_3}{\lambda^\gamma + 2\mu^\gamma}, \\
 A_{2323}^\gamma &= A_{3223}^\gamma = \frac{b_2}{\alpha^\gamma + \mu^\gamma}, \\
 A_{1313}^\gamma &= A_{3113}^\gamma = \frac{b_1}{\alpha^\gamma + \mu^\gamma}, \\
 A_{2332}^\gamma &= \frac{\alpha^\gamma - \mu^\gamma}{\alpha^\gamma + \mu^\gamma} + \frac{b_2}{\alpha^\gamma + \mu^\gamma} \left\langle \frac{\mu - \alpha}{\alpha + \mu} \right\rangle, \\
 A_{1331}^\gamma &= \frac{\alpha^\gamma - \mu^\gamma}{\alpha^\gamma + \mu^\gamma} + \frac{b_1}{\alpha^\gamma + \mu^\gamma} \left\langle \frac{\mu - \alpha}{\alpha + \mu} \right\rangle.
 \end{aligned} \tag{21}$$

In the above relations, we have introduced the redundant notation

$$\begin{aligned}
 b_3 &:= \left(\left\langle \frac{1}{\lambda + 2\mu} \right\rangle + \frac{1}{\ell_3} K_3^{-1} \right)^{-1} = C_{3333}^*, \\
 b_\beta &:= \left(\left\langle \frac{1}{\alpha + \mu} \right\rangle + \frac{1}{\ell_3} K_\beta^{-1} \right)^{-1} = C_{\beta 3 \beta 3}^*, \quad \text{no sum on } \beta = 1, 2,
 \end{aligned} \tag{22}$$

to highlight the dependence of the strain concentration tensor on the interface parameters K_i . Analogous relations can be provided for the curvature concentration tensor \tilde{A}_{ijpq}^γ with interface stiffness Q_i .

It is easy to verify that, considering a perfect interface by letting K_i tend to infinity, the strain concentration tensors verify $V_1 A_{ijpq}^1 + V_2 A_{ijpq}^2 = I_{ijpq}$. Given Eq. (17), the inspection of the non-vanishing components of the tensors A_{ijpq}^γ indicates that a macroscopic strain with non-vanishing normal component \bar{e}_{ii} (no sum on i) will induce concentration only on the local strain normal component e_{33} , i.e. $e_{33} = A_{33ii}^\gamma \bar{e}_{ii}$. Moreover, due to the non-symmetry of the strain concentration tensor, the shear components $\bar{e}_{3\alpha}$ and $\bar{e}_{\alpha 3}$ will induce concentration only on the local shear strains $e_{3\alpha}$, i.e. $e_{3\alpha} = A_{\alpha 3 \alpha 3}^\gamma \bar{e}_{3\alpha}$ and $e_{\alpha 3} = A_{\alpha 3 \alpha 3}^\gamma \bar{e}_{\alpha 3}$ (no sum on α). This is due to the laminated structure of the composite and the assumed material symmetry assumptions, i.e. the centro-symmetric isotropy of the adherents and the choice of diagonal matrices $K_{ij}(Q_{ij})$.

To better evaluate the local deformation of the laminated composite, it is interesting to compute the jumps of the displacements and microrotations fields at the interface between the two adherent laminae in terms of the macroscopic deformation. Using Eqs. (5) and (17), the jumps are

$$\begin{aligned} \llbracket u_i \rrbracket(\mathbf{x}) &= K_{ij}^{-1} C_{jlmn}^\gamma A_{mnpq}^\gamma \bar{e}_{qp}(\mathbf{x}) n_l, \\ \llbracket \omega_i \rrbracket(\mathbf{x}) &= Q_{ij}^{-1} D_{jlmn}^\gamma \tilde{A}_{mnpq} \tilde{\psi}_{qp}(\mathbf{x}) n_l. \end{aligned} \quad (23)$$

One can introduce a displacement jump concentration tensor (F_{ipq}) and a microrotation jump concentration tensor (\tilde{F}_{ipq}), with $n_3 = 1$ and $n_\alpha = 0$, such that

$$\llbracket u_i \rrbracket(\mathbf{x}) = F_{ipq} \bar{e}_{qp}(\mathbf{x}), \quad \llbracket \omega_i \rrbracket(\mathbf{x}) = \tilde{F}_{ipq} \tilde{\psi}_{qp}(\mathbf{x}). \quad (24)$$

Substituting the expressions of C_{jlmn}^γ and A_{mnpq}^γ given by Eqs. (12) and (20), respectively, one obtains that

$$(F_{ipq}) = \begin{pmatrix} 0 & 0 & 0 & 0 & F_{113} & 0 & 0 & F_{131} & 0 \\ 0 & 0 & 0 & F_{223} & 0 & 0 & F_{232} & 0 & 0 \\ F_{311} & F_{322} & F_{333} & 0 & 0 & 0 & 0 & 0 & 0 \end{pmatrix}, \quad (25)$$

with non-vanishing components given by the relations

$$\begin{aligned} F_{\beta\beta 3} &= K_\beta^{-1} \left(\frac{1}{\ell_3} K_\beta^{-1} + \left\langle \frac{1}{\alpha + \mu} \right\rangle \right)^{-1} = b_\beta K_\beta^{-1}, \\ F_{\beta 3 \beta} &= F_{\beta\beta 3} \left\langle \frac{\mu - \alpha}{\alpha + \mu} \right\rangle, \\ F_{333} &= K_3^{-1} \left(\frac{1}{\ell_3} K_3^{-1} + \left\langle \frac{1}{\lambda + 2\mu} \right\rangle \right)^{-1} = b_3 K_3^{-1}, \\ F_{3\beta\beta} &= F_{333} \left\langle \frac{\lambda}{\lambda + 2\mu} \right\rangle. \end{aligned} \quad (26)$$

Analogous form and relations can be obtained for the tensor (\tilde{F}_{ipq}) and its components by substituting the tensor components C_{ijkl} (i.e. the material parameters λ , μ and α) with D_{ijkl} (i.e. β , κ and ϵ), and K_i with Q_i . Notably, the limit of $\llbracket u_i \rrbracket$ ($\llbracket \omega_i \rrbracket$) is zero as K_i (Q_i) approaches infinity, and one recovers the case of perfect contact between the adherents.

Considering the stress and couple stress tensors, using the constitutive relations between the stress and strain, and couple stress and curvature at the macro- and micro-scale and relation (Eq. (17)), one can infer that:

$$\begin{aligned} \sigma_{ji} &= C_{ijpq} e_{qp} = C_{ijpq} A_{pqhk} \bar{e}_{kh} = C_{ijpq} A_{pqhk} S_{hkrs}^* \bar{\sigma}_{sr}, \\ \mu_{ji} &= D_{ijpq} \psi_{qp} = D_{ijpq} \tilde{A}_{pqhk} \tilde{\psi}_{kh} = D_{ijpq} \tilde{A}_{pqhk} \tilde{S}_{hkrs}^* \tilde{\mu}_{sr}, \end{aligned} \quad (27)$$

giving the following relation for the stress and couple stress concentration tensors:

$$B_{ijrs} := C_{ijpq} A_{pqhk} S_{hkrs}^*, \quad \tilde{B}_{ijrs} := D_{ijpq} \tilde{A}_{pqhk} \tilde{S}_{hkrs}^*. \quad (28)$$

Using the Voigt's notation, the 9×9 -matrix form of the stress concentration tensor takes the following form:

$$(B_{ijpq}^*) = \begin{pmatrix} B_{1111}^\gamma & B_{1122}^\gamma & B_{1133}^\gamma & 0 & 0 & 0 & 0 & 0 & 0 \\ B_{2211}^\gamma & B_{2222}^\gamma & B_{2233}^\gamma & 0 & 0 & 0 & 0 & 0 & 0 \\ 0 & 0 & 1 & 0 & 0 & 0 & 0 & 0 & 0 \\ 0 & 0 & 0 & 1 & 0 & 0 & 0 & 0 & 0 \\ 0 & 0 & 0 & 0 & 1 & 0 & 0 & 0 & 0 \\ 0 & 0 & 0 & 0 & 0 & B_{1212}^\gamma & 0 & 0 & B_{1221}^\gamma \\ 0 & 0 & 0 & B_{3223}^\gamma & 0 & 0 & B_{3232}^\gamma & 0 & 0 \\ 0 & 0 & 0 & 0 & B_{3113}^\gamma & 0 & 0 & B_{3131}^\gamma & 0 \\ 0 & 0 & 0 & 0 & 0 & B_{2112}^\gamma & 0 & 0 & B_{2121}^\gamma \end{pmatrix}, \quad (29)$$

where the non-vanishing components are:

$$\begin{aligned} B_{1111}^\gamma &= B_{2222}^\gamma = \frac{\mu^\gamma \left(\lambda^\gamma \left\langle \frac{\mu(3\lambda+4\mu)}{\lambda+2\mu} \right\rangle + 4\mu^\gamma \left\langle \frac{\mu(\lambda+\mu)}{\lambda+2\mu} \right\rangle \right)}{\langle \mu \rangle (\lambda^\gamma + 2\mu^\gamma) \left\langle \frac{\mu(3\lambda+2\mu)}{\lambda+2\mu} \right\rangle}, \\ B_{1122}^\gamma &= B_{2211}^\gamma = -\frac{2\mu^\gamma \left(\lambda^\gamma \left\langle \frac{\mu^2}{\lambda+2\mu} \right\rangle + \mu^\gamma \left\langle \frac{\mu\lambda}{\lambda+2\mu} \right\rangle \right)}{\langle \mu \rangle (\lambda^\gamma + 2\mu^\gamma) \left\langle \frac{\mu(3\lambda+2\mu)}{\lambda+2\mu} \right\rangle}, \\ B_{1133}^\gamma &= B_{2233}^\gamma = \frac{\lambda^\gamma \left\langle \frac{\mu(3\lambda+2\mu)}{\lambda+2\mu} \right\rangle - \mu^\gamma (2\mu^\gamma + 3\lambda^\gamma) \left\langle \frac{\lambda}{\lambda+2\mu} \right\rangle}{(\lambda^\gamma + 2\mu^\gamma) \left\langle \frac{\mu(3\lambda+2\mu)}{\lambda+2\mu} \right\rangle}, \\ B_{1212}^\gamma &= B_{2121}^\gamma = \frac{1}{2} \left(\frac{\mu^\gamma}{\langle \mu \rangle} + \frac{\alpha^\gamma}{\langle \alpha \rangle} \right), \\ B_{3223}^\gamma &= B_{3113}^\gamma = \frac{(\mu^\gamma - \alpha^\gamma) \left\langle \frac{\alpha\mu}{\mu+\alpha} \right\rangle - \alpha^\gamma \mu^\gamma \left\langle \frac{\mu-\alpha}{\mu+\alpha} \right\rangle}{(\alpha^\gamma + \mu^\gamma) \left\langle \frac{\alpha\mu}{\mu+\alpha} \right\rangle}, \\ B_{1221}^\gamma &= B_{2112}^\gamma = \frac{1}{2} \left(\frac{\mu^\gamma}{\langle \mu \rangle} - \frac{\alpha^\gamma}{\langle \alpha \rangle} \right), \\ B_{3232}^\gamma &= B_{3131}^\gamma = \frac{\alpha^\gamma \mu^\gamma}{(\mu^\gamma + \alpha^\gamma) \left\langle \frac{\mu-\alpha}{\mu+\alpha} \right\rangle}. \end{aligned} \quad (30)$$

A long but straightforward calculation shows that the stress concentration tensor verifies the condition $V_1 B_{ijpq}^1 + V_2 B_{ijpq}^2 = I_{ijpq}$. Concerning the concentration tensor of the micropolar couple stress, similar relations can be obtained by substituting the tensor components C_{ijkl} (i.e. the material parameters λ , μ and α) with D_{ijkl} (i.e. β , κ and ϵ). Considering the expression of the stress concentration tensor, we first note that the presence of the unit components follows from the continuity of the traction vector at the interface between the adherent laminae, cf. Eq. (5). Next, the application of a macroscopic in-plane stress $\bar{\sigma}_{\tau\sigma}$ produces a stress concentration on the corresponding in-plane microscopic stresses $\sigma_{\beta\alpha} = B_{\alpha\beta\sigma\tau}^* \bar{\sigma}_{\tau\sigma}$. An equivalent concentration can be induced by applying $\bar{\sigma}_{33}$, i.e., $\sigma_{11} = \sigma_{22} = B_{1133}^* \bar{\sigma}_{33}$. Furthermore, due to the non-symmetry of the strain concentration tensor, the shear stress components $\bar{\sigma}_{3\alpha}$ and $\bar{\sigma}_{\alpha 3}$ will induce concentration only on the local shear stress $\sigma_{\alpha 3}$, i.e. $\sigma_{\alpha 3} = B_{3\alpha\alpha}^* \bar{\sigma}_{3\alpha}$ and $\sigma_{\alpha 3} = B_{3\alpha 3}^* \bar{\sigma}_{\alpha 3}$ (no sum on α).

Notably, while the components of the strain concentration tensors are always well-defined with respect to the volume fractions of the adherents, the components of the stress concentration tensors may be not, due to the vanishing of the averages

$$\left\langle \frac{\mu(3\lambda + 2\mu)}{\lambda + 2\mu} \right\rangle, \quad \left\langle \frac{\alpha\mu}{\mu + \alpha} \right\rangle, \quad \langle \mu \rangle, \quad \langle \alpha \rangle, \quad (31)$$

at some values of the volume fraction V_1 . The first of these averages enters the engineering moduli E_1^* , E_3^* , the second one the shear moduli G_{23}^* , G_{13}^* , $G_{32}^* = G_{31}^*$, and the last two ones the shear moduli $G_{12}^* = G_{21}^*$. The vanishing of one or more of these engineering elastic constants and the analogous engineering micropolar constants signals the indefiniteness of the compliance tensor. This in turn implies that the last step in Eq. (27) is no longer valid, and one should be content with calculating the local stress in terms of the average macroscopic strain. In the next Section, we provide a numerical example where some engineering constants vanish at some specific values of V_1 , and, as a result, components of the micropolar couple stress tensor (\tilde{B}_{ijpq}^*) are found to diverge at these values of V_1 .

Interestingly enough, the components of the stress concentration tensor turn out to be independent of the imperfection parameters K_i , Q_i implying that a macroscopic stress will induce local stress concentration independently of the properties of the contact surface. In the next Section, we provide an example showing that the independence of the stress concentration tensors of the imperfection parameters K_i , Q_i is not unexpected, and it is due to the assumption of the particular imperfect contact model between the laminae, i.e. the layer of springs.

In the proposed example, we consider a simplified setting, a laminate made of two laminae composed of linear elastic materials and

in perfect contact. It is known that imperfect contact conditions of the type (5) can be viewed as arising from the limit behavior of a weak layer, i.e. a very thin layer made of a soft material, cf. [18–20]. Thus, using the explicit solution proposed by Glüge and Kalisch in [46] for an elastic bi-laminated composite, we show that when one lamina becomes thin and soft, modeling a thin layer of spring, the stress concentration tensor in the other lamina becomes independent of the elasticity properties of the weak lamina. The present analysis based on AHM generalizes the example of the bi-layered laminate to the case of a micropolar elastic multi-laminate.

Finally, it is noteworthy that the independence of stress concentration tensors of the properties of the imperfect contact surface impacts the modeling strategies adopted for the composite laminate. This aspect will be discussed in the Conclusion section.

5. An example: a bi-laminated elastic composite with a weak layer

In this Section, we restrict ourselves to the simpler case considered by Glüge and Kalisch in [46] of a bi-layered laminate composed of linear elastic materials with elasticity tensors \mathbf{C}^γ and volume fractions V_γ ($\gamma = 1, 2$), such that $V_1 + V_2 = 1$. Let us denote with \mathbf{n} , the unit normal vector to the interface between the two layers, oriented outward from the layer with $\gamma = 2$ to the layer with $\gamma = 1$, and we take \mathcal{A}^γ ($\gamma = 1, 2$) as the second-order acoustic tensors associated with the two layers, such that $\mathcal{A}_{ir}^\gamma := C_{ijrs}^\gamma n_j n_s$. In addition, let \mathcal{Z} be the second-order tensor such that $\mathcal{Z}^{-1} = V_2 \mathcal{A}^1 + V_1 \mathcal{A}^2$, and \mathbb{Z}^S be the symmetric part of the fourth-order tensor defined as $\mathbb{Z}_{jirs} := n_j \mathcal{Z}_{ir} n_s$.

In [46], it is shown that the effective stiffness \mathbf{C}^* of the laminate takes the form

$$\mathbf{C}^* = \langle \mathbf{C} \rangle - V_1 V_2 \Delta \mathbf{C} \mathbb{Z}^S \Delta \mathbf{C}, \quad (32)$$

with $\Delta \mathbf{C} := \mathbf{C}^1 - \mathbf{C}^2$. The Eq. (32) shows that the effective stiffness is given by Voigt's bound diminished by a negative semi-definite term.

The strain concentration tensors in the two layers are

$$\mathbf{A}^1 = \mathbb{I}^S - V_2 \mathbb{Z}^S \Delta \mathbf{C}, \quad \mathbf{A}^2 = \mathbb{I}^S + V_1 \mathbb{Z}^S \Delta \mathbf{C}, \quad (33)$$

where \mathbb{I}^S is the fourth-order identity tensor on symmetric second-order tensors and the stress concentration tensors are calculated as

$$\mathbf{B}^1 = \mathbf{C}^1 \mathbf{A}^1 \mathbf{S}^*, \quad \mathbf{B}^2 = \mathbf{C}^2 \mathbf{A}^2 \mathbf{S}^*, \quad (34)$$

where $\mathbf{S}^* = \mathbf{C}^{*-1}$ denotes the effective compliance tensor.

Now, let us suppose that the layer, labeled with $\gamma = 2$, is a thin, soft layer, so that

$$V_2 = \varepsilon V_0, \quad \mathbf{C}^2 = \varepsilon \mathbf{C}_0, \quad (35)$$

with V_0 a constant and \mathbf{C}_0 a constant elasticity tensor, both independent of the small parameter ε , [18–20]. In the sequel, the index 0 will be taken to denote quantities independent of ε . Substituting the relations (35) into the expressions of the tensors \mathcal{A}^2 , \mathcal{Z} and \mathbb{Z}^S gives

$$\mathcal{A}^2 = \varepsilon \mathcal{A}_0, \quad \mathcal{Z} = \varepsilon^{-1} \mathcal{Z}_0, \quad \mathbb{Z}^S = \varepsilon^{-1} \mathbb{Z}_0^S. \quad (36)$$

Then, substituting these results into Eqs. (32) and (33), we obtain the following approximations for the effective stiffness and the strain concentration tensor of layer 1:

$$\mathbf{C}^* = V_1 \mathbf{C}^1 (\mathbb{I}^S - V_0 \mathbb{Z}_0^S \mathbf{C}^1) + \varepsilon V_1 V_0 (\mathbf{C}^1 \mathbb{Z}_0^S \mathbf{C}_0 + \mathbf{C}_0 \mathbb{Z}_0^S \mathbf{C}^1) + o(\varepsilon), \quad (37)$$

$$\mathbf{A}^1 = \mathbb{I}^S - V_0 \mathbb{Z}_0^S \mathbf{C}^1 + \varepsilon V_0 \mathbb{Z}_0^S \mathbf{C}_0 + o(\varepsilon), \quad (38)$$

and replacing the latter ones into Eq. (34), we find that

$$\begin{aligned} \mathbf{B}^1 &= V_1^{-1} \mathbb{I}^S + \varepsilon V_1^{-1} \mathbf{C}_0 (\mathbb{I}^S - (\mathbb{I}^S - V_0 \mathbb{Z}_0^S \mathbf{C}^1)^{-1}) (\mathbf{C}^1)^{-1} + o(\varepsilon) \\ &= \mathbb{I}^S + \varepsilon (V_0 \mathbb{I}^S + \mathbf{C}_0 (\mathbb{I}^S - (\mathbb{I}^S - V_0 \mathbb{Z}_0^S \mathbf{C}^1)^{-1}) (\mathbf{C}^1)^{-1}) + o(\varepsilon), \end{aligned} \quad (39)$$

being $V_1^{-1} = 1 + \varepsilon V_0 + o(\varepsilon)$.

This shows that at the zero-th order in ε the stress concentration tensor becomes independent of the elasticity properties of the weak

Table 1

Material parameters of the two micropolar layers constituting the periodic laminate [47].

Materials data	λ (MPa)	μ (MPa)	α (MPa)	β (N)	κ (N)	ϵ (N)
SyF	2097.0	1033.0	114.8	-2.91	4.364	-0.133
PUF	762.7	104.0	4.333	-26.65	39.98	4.504

layer, but it does depend on them at the first order in ε . In [18–20], it is shown that an imperfect interface of spring-type can be seen as the limit of a weak layer, in the sense specified by Eq. (35), as ε goes to zero. In other words, the spring-type interface is the order zero interface model that better approximates the mechanical behavior of a very thin soft layer. At higher orders in ε , the form of the interface law is more elaborate and can be found in [20].

Thus, the result obtained in Section 4, namely, the stress concentration tensors of a two-layer micropolar laminate with imperfect contact conditions are independent of the stiffness parameters of the spring layer, is not unexpected, and it can be viewed as a generalization to the case of micropolar elasticity of the particular (pure elastic) case illustrated in this Section when only the terms at order zero in ε are retained. Based on these results, we also expect that a homogenization analysis for a composite incorporating a higher order interface condition would give stress and couple stress fields dependent on the imperfect interface parameters.

6. Numerical results

In this Section, we numerically study the effect of a uniform imperfect interface on the local values of strain and stress in a centrosymmetric bi-laminated composite with isotropic constituents employing the strain and stress concentration tensors defined in Section 4. For our computations, we assume the layer 1 to be made of SyF (syntactic foam - hollow glass spheres in epoxy resin) and the layer 2 to be made of PUF (dense polyurethane foam). The material properties for SyF and PUF are taken from [47], and they are listed in Table 1.

Figs. 2 and 3 show the variation of the components of the strain and curvature concentration tensors, respectively, with respect to the volume fraction of SyF, V_1 . In view of (17), the components of (A_{ijpq}) and (\tilde{A}_{ijpq}) represent local strain and curvature components, respectively, normalized with respect to single applied uniform macroscopic strain and curvature components. Black and gray curves represent normalized local strains and curvatures in SyF and in PUF, respectively. Continuous, dashed, dash-dotted, and dotted lines refer to different values of the imperfection parameters $K := K_i$ [N/m³], and $Q := Q_i$ [N/m], $i = 1, 2, 3$, taken to range between 10^6 and 10^{12} . Note that, in view of the results presented in [20,43,44], the values chosen for K would correspond to a soft thin elastic layer with modulus/thickness ratio varying from 10^{-3} MPa/mm to 10^3 MPa/mm. For the micropolar coefficients Q , they would correspond to a soft thin layer with micropolar modulus/thickness ratio varying from 10^3 N/mm to 10^9 N/mm [28]. For the cell length ℓ_3 , a fixed value of 10^{-6} m is assumed.

The plots in Fig. 2 indicate that (the absolute value of) the strain is locally larger in PUF than in SyF. This is consistent with the larger values of the elasticity constants of SyF compared to PUF (cf. Table 1), indicating that SyF is more rigid than PUF. The opposite occurs for the micro-polar constants β , κ and ϵ , whose absolute values are larger in PUF than in SyF, thus causing (the absolute value of) the curvature to be always larger in SyF, as illustrated in Fig. 3. The effect of the imperfection parameters is similar in both Figures: larger values of K and Q are associated with greater absolute values of normalized local strain and curvature.

Figs. 4 and 5 show the variation of the displacement and micro-rotation jumps, respectively, with the volume fraction of SyF, V_1 , for different values of the interface parameters.

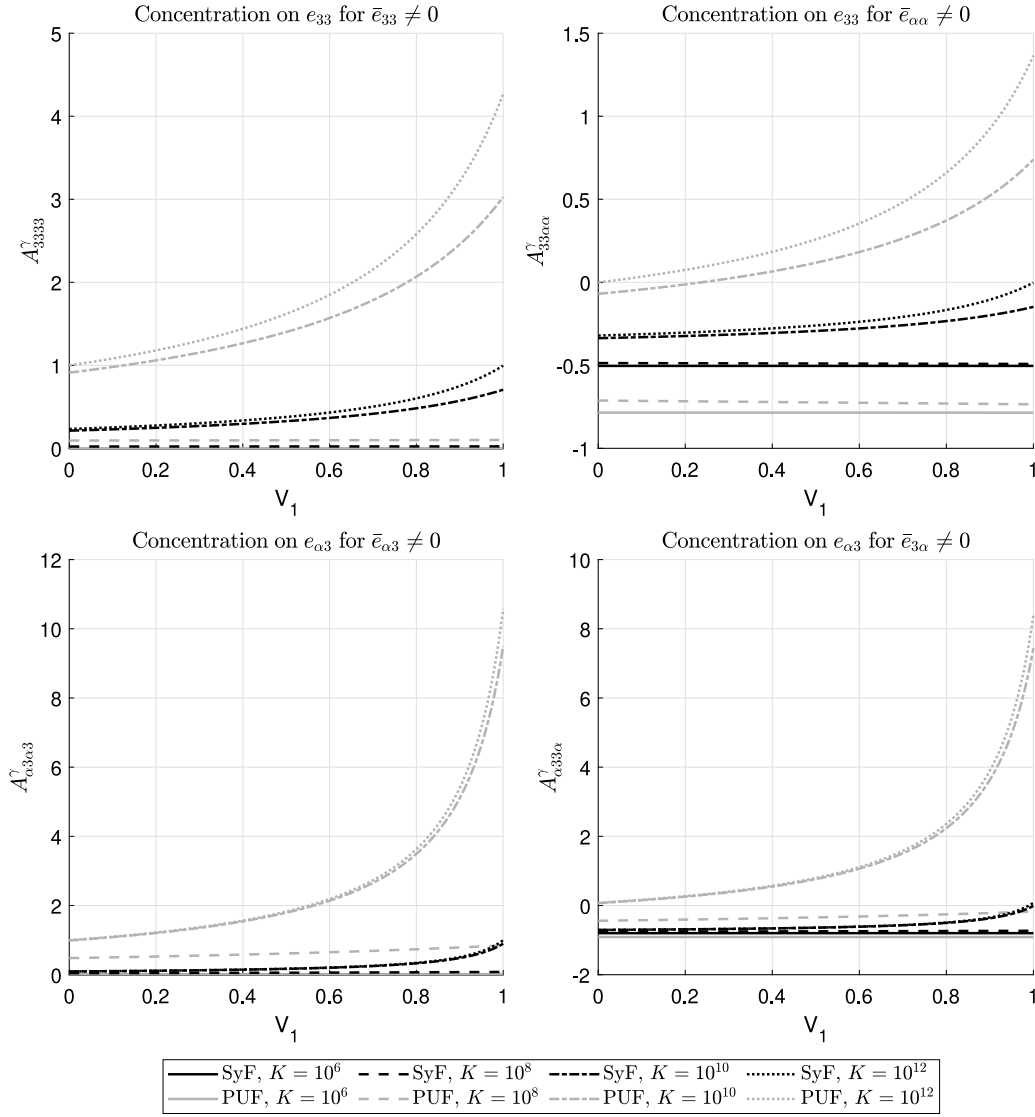


Fig. 2. Effect of the volume fraction of SyF, V_1 , and of interface parameters $K := K_i, i = 1, 2, 3$, on the variation of normalized local strain components $A_{3333} = e_{33}/\bar{e}_{33}$, $A_{33aa} = e_{33}/\bar{e}_{aa}$, $A_{a3a3} = e_{a3}/\bar{e}_{a3}$, and $A_{a33a} = e_{a3}/\bar{e}_{3a}$, for single applied uniform macroscopic deformation components \bar{e}_{33} , \bar{e}_{aa} , \bar{e}_{a3} , and \bar{e}_{3a} , respectively, in SyF (black lines) and PUF (gray lines).

The plots of Figs. 4 and 5 show that smaller values of (the absolute value of) the jumps are associated with increased values of the interface parameters. Together, Figs. 2, 3, 4 and 5 indicate that, as expected, the stiffer the interface, the greater the strain and curvature localization on the layers and the smaller the displacement and microrotation jumps at the interface. Interestingly, the normalized strain and curvature components e'_{33}/\bar{e}_{aa} and $\psi'_{33}/\bar{\psi}_{aa}$ may be positive, indicating that the layers locally exhibit an auxetic behavior, i.e. they expand along the 3-axis when the composite is macroscopically uniaxially stretched along the 1-axis or 2-axis, and vice versa. Similar considerations apply to the normalized components e'_{a3}/\bar{e}_{3a} and $\psi'_{a3}/\bar{\psi}_{3a}$.

Figs. 6 and 7 show the variation of the normal and tangential local stress concentration components, respectively, with respect to the volume fraction of SyF, V_1 , while Figs. 8 and 9 show the variation of the normal and tangential local couple-stress concentration components. As before, black and gray curves refer to components in SyF and PUF, respectively.

These plots do not depend on the interface parameters, K and Q , as shown in the previous Sections. The trends of the plots indicate that SyF, the more rigid material, absorbs a larger amount of the applied stress, as expected. The situation is reversed for the couple-stress,

being PUF the stiffer material for the micropolar part. The couple-stress concentration is also found to exhibit an asymptotic behavior at specific volume fractions of SyF. In particular, as shown in Figs. 8 and 9, the local couple-stress components \bar{B}'_{aaaa} , $\bar{B}'_{\alpha\alpha\beta\beta}$, and $\bar{B}'_{\alpha\alpha 33}$ exhibit an asymptotic behavior at $V_1 \approx 0.83331$, the component $\bar{B}'_{3a\alpha 3}$ at $V_1 \approx 0.96722$, and the components $\bar{B}'_{\alpha\beta\alpha\beta}$ and $\bar{B}'_{\alpha\beta\beta\alpha}$ at $V_1 \approx 0.97132$. At these three particular values of V_1 , the averages

$$\left\langle \frac{\kappa(3\beta + 2\kappa)}{\beta + 2\kappa} \right\rangle, \quad \left\langle \frac{\epsilon\kappa}{\kappa + \epsilon} \right\rangle, \quad \langle \epsilon \rangle \quad (40)$$

vanish, thus determining the observed asymptotic behavior of the couple-stress components. It is interesting to notice that the effective engineering torsional Young's modulus \bar{E}_3^* (and, thus, the twist Poisson's ratio $\bar{\nu}_{32}^*$) is also found to vanish at $V_1 \approx 0.83331$, due to the vanishing of the first average in (40), cf. the first and last plot of Figure 19.3 in [40]. Similarly, the effective engineering torsional shear modulus \bar{G}_{13}^* is found to vanish at $V_1 \approx 0.96722$, due to the vanishing of the second average in (40), cf. the middle plot of Figure 19.3 in [40]. Accordingly, the engineering shear torsional elastic modulus \bar{G}_{12}^* is expected to vanish at $V_1 \approx 0.97132$, due to the vanishing of the third and last average in Eq. (40). The average $\langle \kappa \rangle$ is never found to vanish for V_1 in $[0, 1]$, thus the asymptotic behavior is not observed in \bar{B}'_{3a3a} .

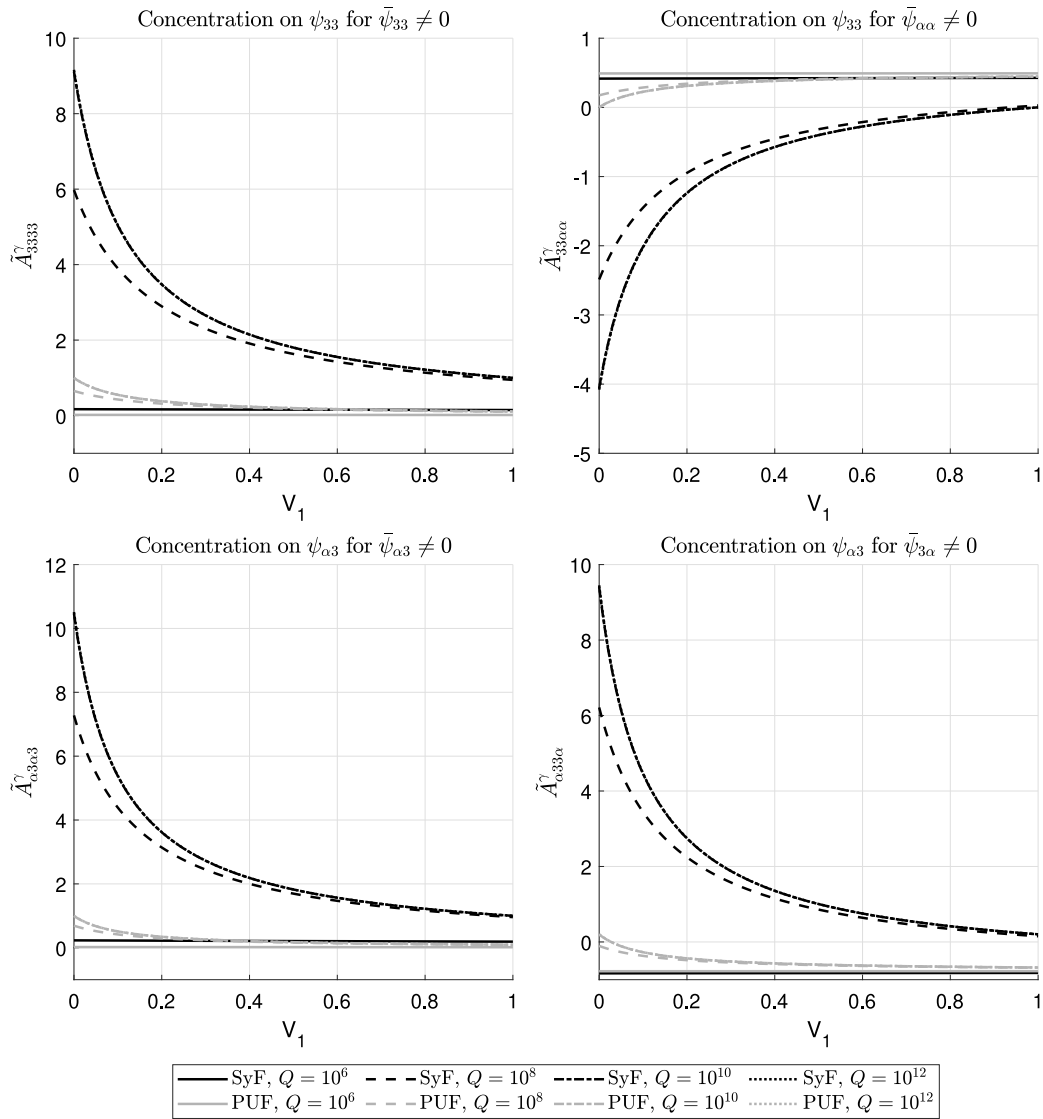


Fig. 3. Effect of the volume fraction of SyF, V_1 , and of interface parameter $Q := Q_i, i = 1, 2, 3$, on the variation of normalized local torsion-curvature components $\tilde{A}_{3333} = \psi_{33}/\bar{\psi}_{33}$, $\tilde{A}_{33\alpha\alpha} = \psi_{33}/\bar{\psi}_{\alpha\alpha}$, $\tilde{A}_{\alpha3\alpha3} = \psi_{\alpha3}/\bar{\psi}_{\alpha3}$, and $\tilde{A}_{\alpha33\alpha} = \psi_{\alpha3}/\bar{\psi}_{3\alpha}$, for single applied uniform macroscopic deformation components $\bar{\psi}_{33}$, $\bar{\psi}_{\alpha\alpha}$, $\bar{\psi}_{\alpha3}$, and $\bar{\psi}_{3\alpha}$, respectively, in SyF (black lines) and PUF (gray lines).

7. Conclusion

This paper investigates the strain, curvature, stress, and couple-stress concentration tensors in the adherents materials of a laminate composed of thin micropolar laminae joined by layers of springs. These concentration tensors link macroscopic averaged quantities (stress/couple-stress and strain/curvature) with their microscopic counterparts.

As expected, the components of the strain and curvature concentration tensors are found to depend on the elasticity constants of the two laminae and the stiffness properties of the spring-type interface. Notably, the components of the stress and couple-stress concentration tensors turn out to depend only on the elastic constants of the two laminae, i.e. they are independent of the elastic properties of the spring-type interface joining the adherents. In Section 5, we show that this result is not unexpected, as it is also found in the simplified setting of a composite laminate composed of identical laminae joined by a soft thin elastic layer.

The independence of the stress concentration tensors of the properties of the imperfect contact surface impacts the modeling strategies adopted for a laminated composite. Indeed, one would expect stress

concentrations to arise as a consequence of interfacial defects. Thus, the results obtained in the present paper could be attributed to the simplicity of the spring-type interface model. In the example proposed in Section 5, taking higher order terms would give a stress concentration tensor depending on the elastic properties of the soft thin layer. This suggests that the modeling design of the laminate can be improved by the introduction of higher order interface laws of the type proposed in [20,43,44,48]. On the other hand, it is known that in the presence of debonding, strain- and stress-driven homogenization approaches lead to different results, cf. [49,50]. The present investigation was based on a displacement approach. It can be conjectured that a homogenization approach based on the expansion of the stress field could lead to different results for the dependence of the stress concentration tensor on the interface parameters. These aspects will be the object of future work.

The primary goal of the paper was to demonstrate how to determine local stress and deformation components from macroscopic quantities using tools from asymptotic homogenization theory. We believe that understanding how material parameters — such as the elastic and micropolar properties of the adherents and interface — affect local

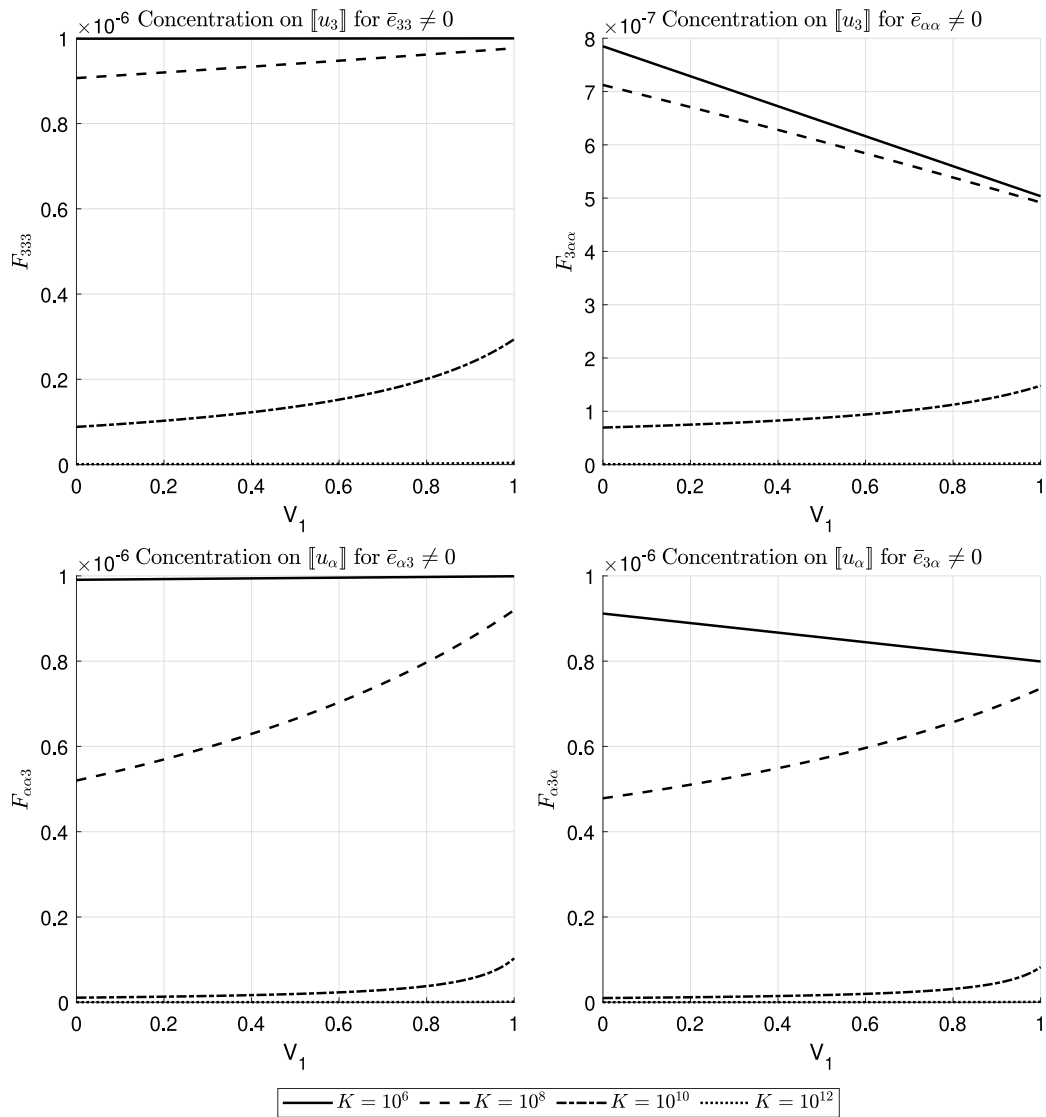


Fig. 4. Effect of the volume fraction of SyF, V_1 , and of interface parameters $K := K_i, i = 1, 2, 3$, on the variation of normalized local displacement jumps $F_{333} = [[u_3]]/\bar{e}_{33}$, $F_{3\alpha\alpha} = [[u_3]]/\bar{e}_{3\alpha}$, $F_{\alpha\alpha 3} = [[u_\alpha]]/\bar{e}_{\alpha 3}$, and $F_{\alpha 3\alpha} = [[u_\alpha]]/\bar{e}_{3\alpha}$, for single applied uniform macroscopic deformation components \bar{e}_{33} , $\bar{e}_{3\alpha}$, $\bar{e}_{\alpha 3}$, and $\bar{e}_{3\alpha}$, respectively, in SyF (black lines) and PUF (gray lines).

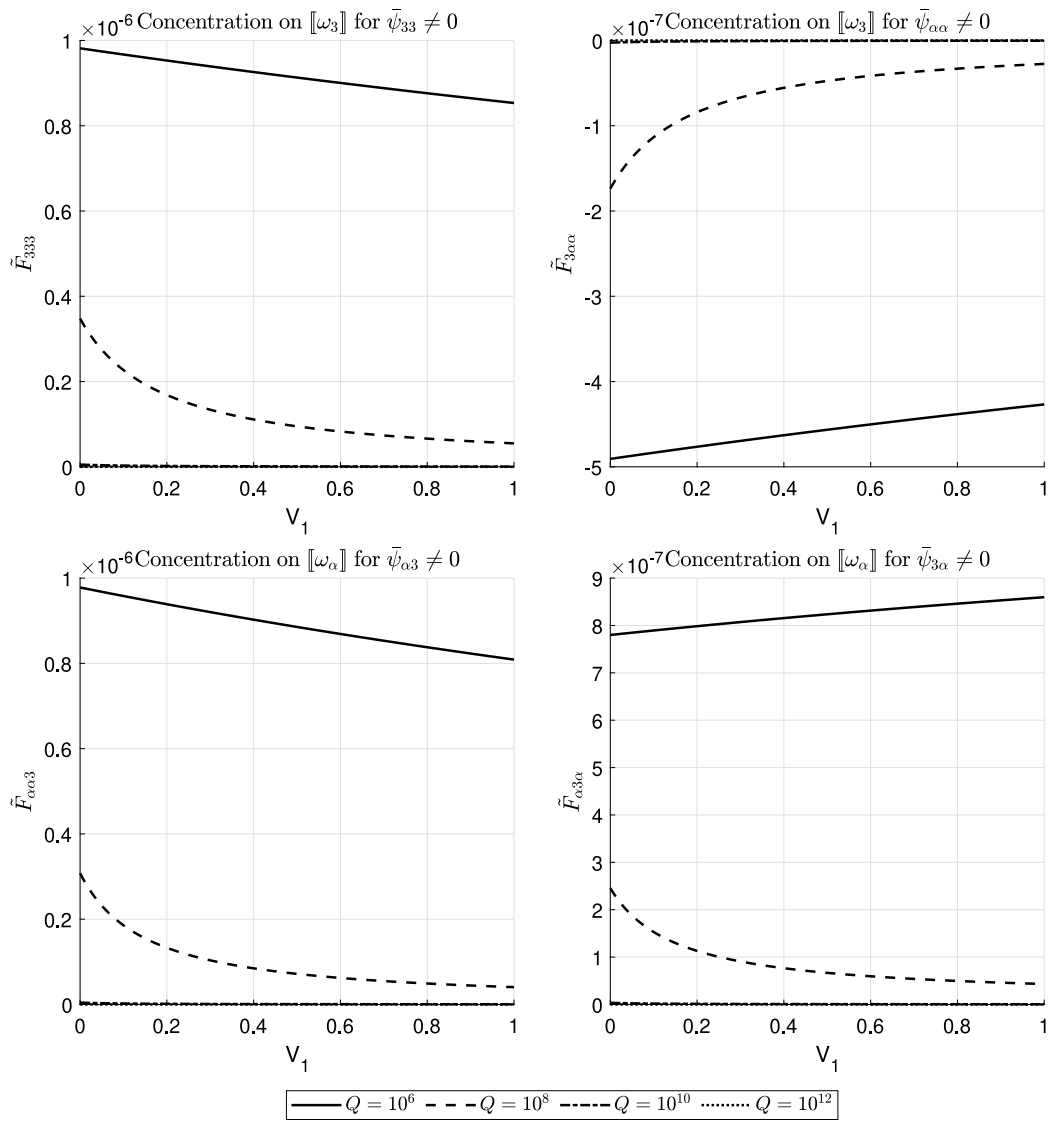


Fig. 5. Effect of the volume fraction of SyF, V_1 , and of interface parameters $Q := Q_i, i = 1, 2, 3$, on the variation of normalized local displacement jumps $\tilde{F}_{333} = \llbracket \omega_3 \rrbracket / \bar{\psi}_{33}$, $\tilde{F}_{3\alpha\alpha} = \llbracket \omega_3 \rrbracket / \bar{\psi}_{33}$, $\tilde{F}_{\alpha\alpha 3} = \llbracket \omega_\alpha \rrbracket / \bar{\psi}_{\alpha 3}$, and $\tilde{F}_{\alpha 3\alpha} = \llbracket \omega_\alpha \rrbracket / \bar{\psi}_{3\alpha}$, for single applied uniform macroscopic deformation components $\bar{\psi}_{33}$, $\bar{\psi}_{33}$, $\bar{\psi}_{\alpha 3}$, and $\bar{\psi}_{3\alpha}$, respectively, in SyF (black lines) and PUF (gray lines).

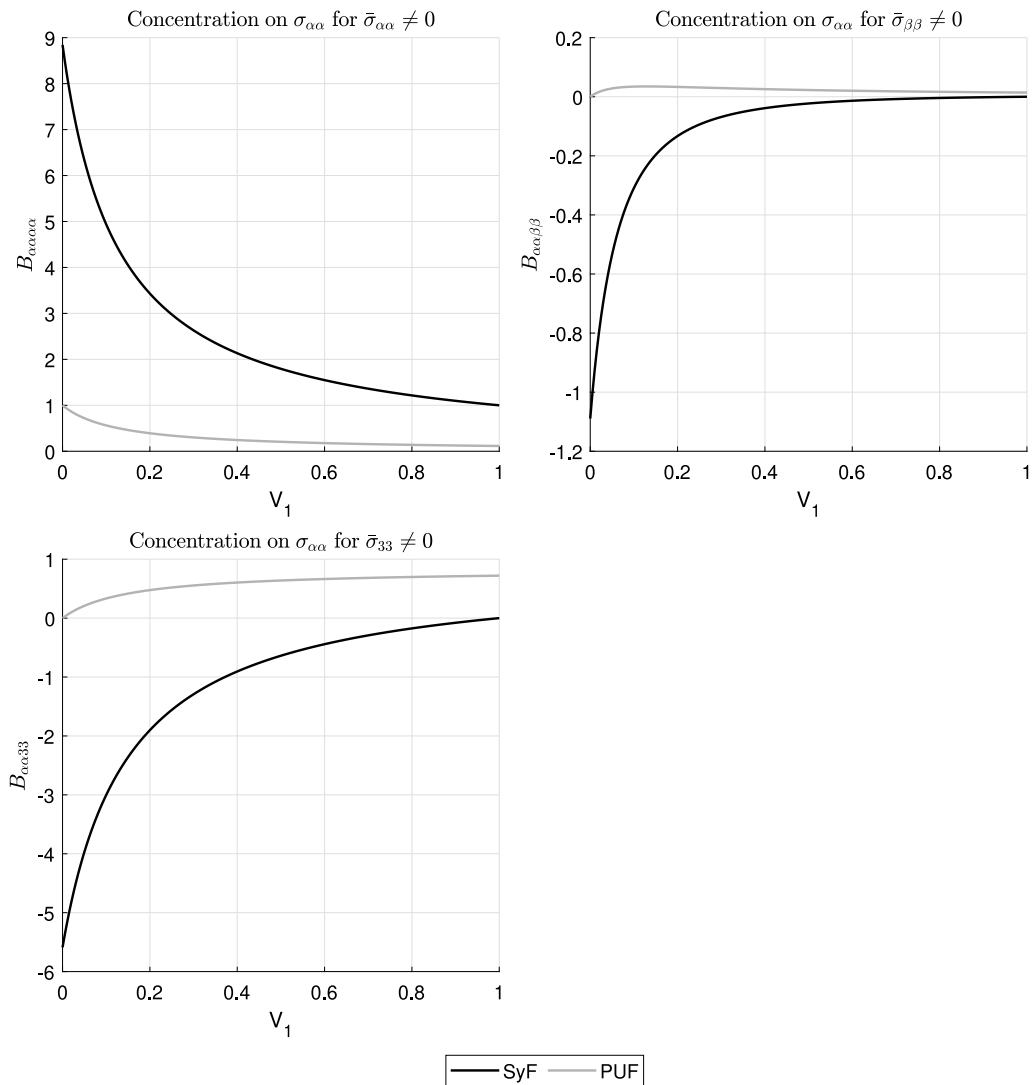


Fig. 6. Effect of the volume fraction of SyF, V_1 , on the variation of normalized local stress components $\sigma_{11}/\bar{\sigma}_{11}$, $\sigma_{11}/\bar{\sigma}_{22}$, and $\sigma_{11}/\bar{\sigma}_{33}$, for applied uniform macroscopic stress components $\bar{\sigma}_{11}$, $\bar{\sigma}_{22}$, $\bar{\sigma}_{33}$, respectively, in SyF (black lines) and PUF (gray lines).

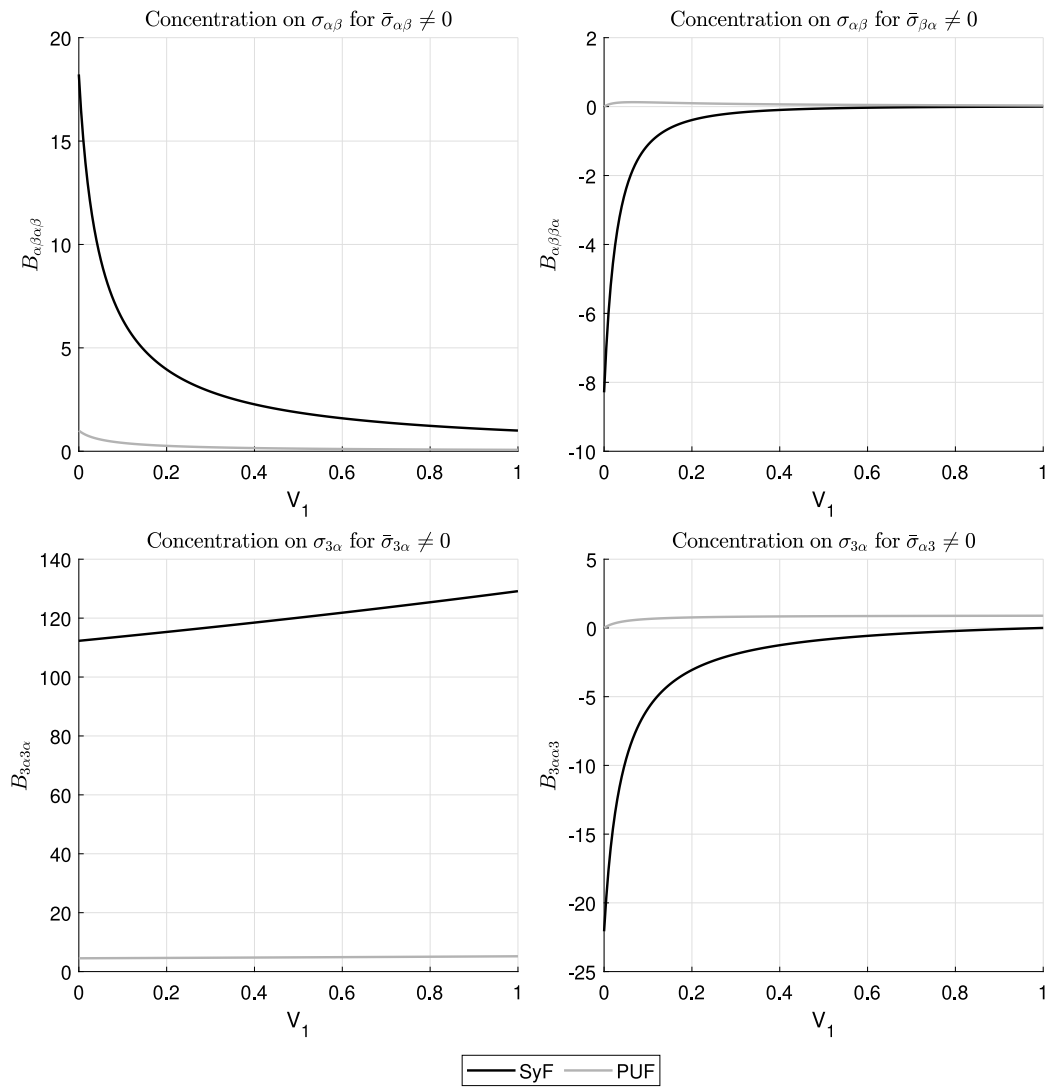


Fig. 7. Effect of the volume fraction of SyF, V_1 , on the variation of normalized local stress components $\sigma_{12}/\bar{\sigma}_{12}$, $\sigma_{12}/\bar{\sigma}_{21}$, $\sigma_{32}/\bar{\sigma}_{23}$, and $\sigma_{32}/\bar{\sigma}_{32}$ for applied uniform macroscopic stress components $\bar{\sigma}_{12}$, $\bar{\sigma}_{21}$, $\bar{\sigma}_{23}$, and $\bar{\sigma}_{32}$, respectively, in SyF (black lines) and PUF (gray lines).

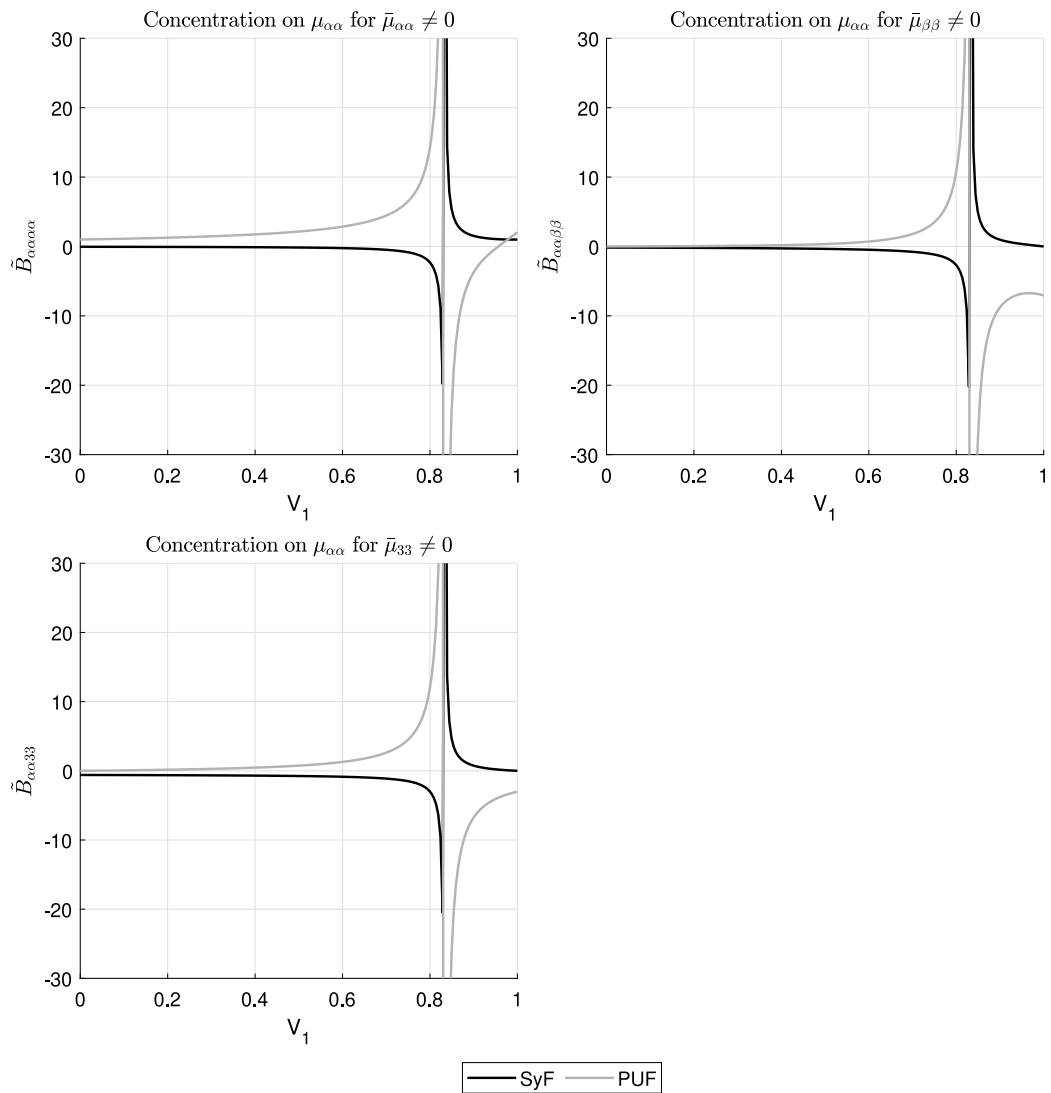


Fig. 8. Effect of the volume fraction of SyF, V_1 , on the variation of normalized local couple-stress components $\mu_{11}/\bar{\mu}_{11}$, $\mu_{11}/\bar{\mu}_{22}$, and $\mu_{11}/\bar{\mu}_{33}$, for applied uniform macroscopic couple-stress components $\bar{\mu}_{11}$, $\bar{\mu}_{22}$, $\bar{\mu}_{33}$, respectively, in SyF (black lines) and PUF (gray lines).

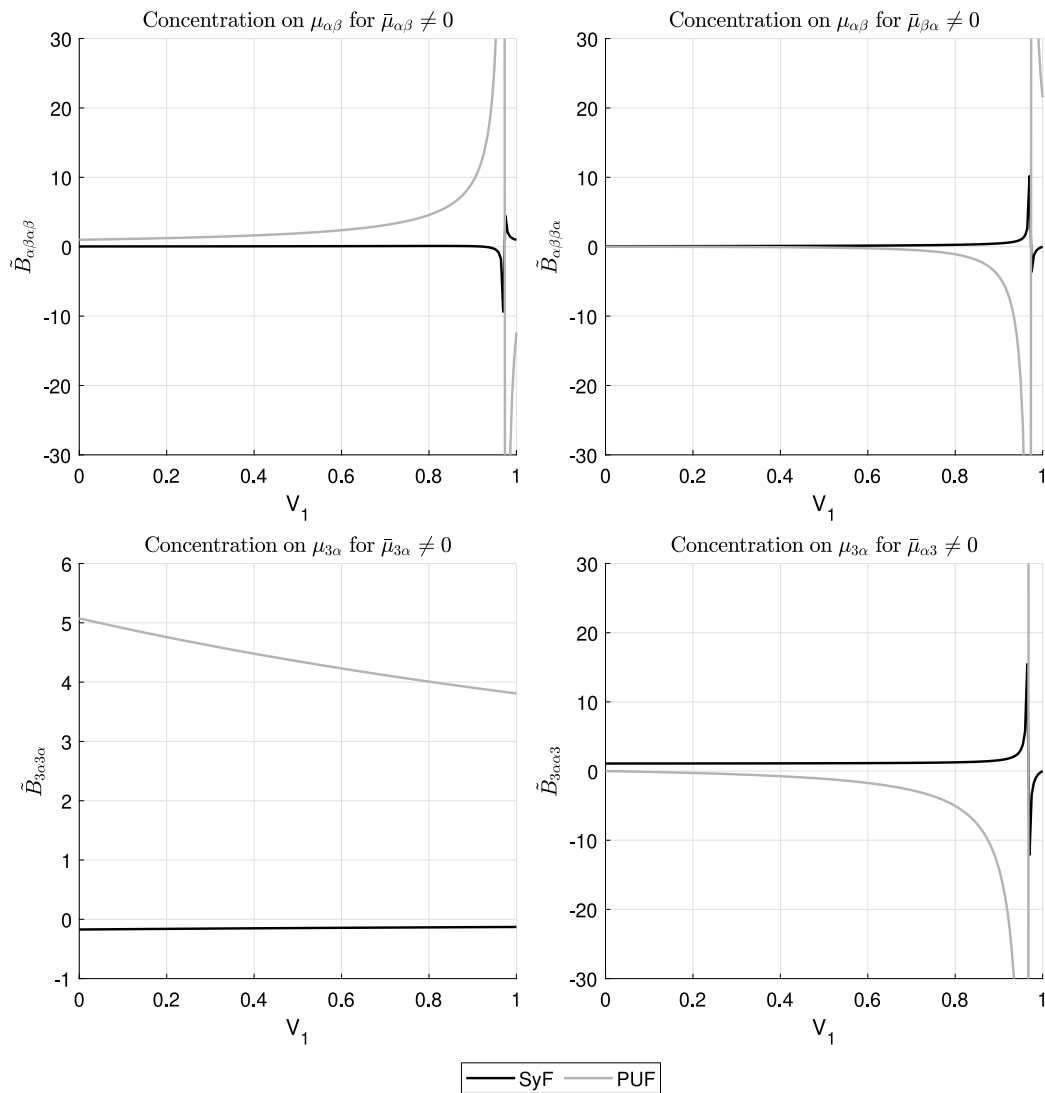


Fig. 9. Effect of the volume fraction of SyF, V_1 , on the variation of normalized local couple-stress components $\mu_{12}/\bar{\mu}_{12}$, $\mu_{12}/\bar{\mu}_{21}$, $\mu_{32}/\bar{\mu}_{23}$, and $\mu_{32}/\bar{\mu}_{32}$ for applied uniform macroscopic stress components $\bar{\mu}_{12}$, $\bar{\mu}_{21}$, $\bar{\mu}_{23}$, and $\bar{\mu}_{32}$, respectively, in SyF (black lines) and PUF (gray lines).

stress and strain components is crucial for developing an effective damage and failure theory, analyzing interlaminar cracks or delamination. However, these topics lie outside the scope of the present work.

CRediT authorship contribution statement

Raffaella Rizzoni: Writing – original draft, Writing – review & editing, Software, Visualization, Validation, Methodology, Investigation, Formal analysis, Conceptualization, Funding acquisition, Project administration. **Michele Serpilli:** Writing – original draft, Writing – review & editing, Software, Validation, Methodology, Investigation, Formal analysis, Conceptualization. **Reinaldo Rodríguez-Ramos:** Writing – review & editing, Validation, Supervision, Methodology, Investigation, Funding acquisition, Formal analysis, Conceptualization. **Yoanh Espinosa-Almeyda:** Writing – review & editing, Validation, Supervision, Methodology. **Frédéric Lebon:** Writing – review & editing, Validation, Supervision, Methodology, Investigation, Funding acquisition. **Maria Letizia Raffa:** Writing – review & editing, Validation, Supervision. **Serge Dumont:** Writing – review & editing, Validation, Supervision.

Declaration of competing interest

The authors declare that they have no known competing financial interests or personal relationships that could have appeared to influence the work reported in this paper.

Acknowledgments

This work was conceived during the visit of RRR at the University of Ferrara in 2022. RRR thanks co-funding of the Departmental Strategic Plan, Department of Engineering, University of Ferrara and Chamada CNPq Nº 09/2023 PQ-2 Produtividade em Pesquisa, processo nº. 307188/2023-0 e ao Edital UFF PROPPi nº . 05/2022. YEA gratefully acknowledges the CONACYT for the postdoctoral scholarship “Estancias Postdoctorales por México para la Formación y Consolidación de Investigadores por México” performed at IIT, UACJ,2022–2024. YEA and RRR are grateful to the support of CONAHCYT Frontiers of Science project numbers CF-2023-G-792 and CF-2023-G-1458. This research has been conducted according to the inspiring scientific principles of the Italian National Group for the Mathematical Physics (GNFM) of the National Institute for Advanced Mathematics (INdAM).

Data availability

No data was used for the research described in the article.

References

- [1] Bensoussan A, Lions JL, Papanicolaou G. Asymptotic analysis for periodic structures. AMS Chelsea Publishing; 2011.
- [2] Chatzigeorgiou G, Meraghni F, Charalambakis N. Multiscale modeling approaches for composites. Elsevier; 2022.
- [3] Hill R. Elastic properties of reinforced solids: some theoretical principles. *J Mech Phys Solids* 1963;11(5):357–72.
- [4] Kalamkarov AL, Andrianov IV, Danishevskyy VV. Asymptotic homogenization of composite materials and structures. *ASME Appl Mech Rev* 2009;62(3):030802.
- [5] Lee H, Lee S, Ryu S. Advancements and challenges of micromechanics-based homogenization for the short fiber reinforced composites. *Multiscale Sci Eng* 2023;5:133–46.
- [6] Milton GW. The theory of composites. Cambridge University Press; 2002.
- [7] Mura T. Micromechanics of defects in solids. 2nd ed. revised ed.. Dordrecht etc. Martinus Nijhoff Publishers; 1987.
- [8] Nemat-Nasser S, Hori M. Micromechanics : Overall properties of heterogeneous materials. Amsterdam ; New York: North-Holland; 1993.
- [9] Pobedrya BE. Mechanics of composite materials [in Russian]. Moscow: Izd-vo MGU; 1984.
- [10] Drago AS, Pindera M. A locally exact homogenization theory for periodic microstructures with isotropic phases. *ASME J Appl Mech* 2008;75(5):051010.
- [11] Lakes R. Experimental microelasticity of two porous solids. *Int J Solids Struct* 1986;22(1):55–63.
- [12] Mogilevskaya SG, Crouch SL, Stolarski HK, Benusiglio A. Equivalent inhomogeneity method for evaluating the effective elastic properties of unidirectional multi-phase composites with surface/interface effects. *Int J Solids Struct* 2010;47:407–18.
- [13] Nazarenko L, Stolarski H. Energy-based definition of equivalent inhomogeneity for various interphase models and analysis of effective properties of particulate composites. *Compos B* 2016;94:82–94.
- [14] Geiss PL, Schumann M. Investigation of the mechanical properties of interphases in adhesively bonded epoxy-aluminum joints by localized micro extensometry. *J Adhes* 2012;88(11–12):941–55.
- [15] Krüeger JK, Possart W, Bactavachalou R, Müller U, Britz T, Sanctuary R, Alnot P. Gradient of the mechanical modulus in glass-epoxy-metal joints as measured by Brillouin microscopy. *J Adhes* 2004;80:585–99.
- [16] Safavi-Ardebili V, Sinclair AN, Spelt JK. Experimental investigation of the interphase in an epoxy-aluminum system. *J Adhes* 1997;62:93–111.
- [17] Firooz S, Steinmann P, Javili A. Homogenization of composites with extended general interfaces: Comprehensive review and unified modeling. *ASME Appl Mech Rev J* 2021;73(4):040802.
- [18] Lebon F, Rizzoni R. Asymptotic analysis of a thin interface: The case involving similar rigidity. *Internat J Engrg Sci* 2010;48:473–86.
- [19] Lebon F, Rizzoni R. Asymptotic behavior of a hard thin linear interphase: An energy approach. *Int J Solids Struct* 2011;48:441–9.
- [20] Rizzoni R, Dumont S, Lebon F, Sacco E. Higher order model for soft and hard elastic interfaces. *Int J Solids Struct* 2014;51:4137–48.
- [21] Budzik M, Jumel J, Shanahan MER. Adhesive compliance effect in mode I separation: Profilometry approach. *Int J Adhes Adhes* 2011;31(3):135–45.
- [22] Mascaro B, Budzik MK, Castaings M, Jumel J, Shanahan MER. Evaluation of adhesive bond Young's modulus during crosslinking using a mechanical method and an ultrasound method. *J Phys: Conf Ser* 2012;353:012006.
- [23] Rizzoni R, Dumont S, Lebon F, Sacco E. Higher order adhesive effects in composite beams. *Eur J Mech A-Solids* 2021;85:104108.
- [24] Cosserat E, Cosserat F. Théorie des corps déformables. In: Cholson OD, editor. *Treatise of physics*. Paris: Hermann; 1909, p. 963–1173.
- [25] Eremeyev VA, Lebedev LP, Altenbach H. Foundations of micropolar mechanics. Springerbriefs in applied sciences and technology - Continuum mechanics, Berlin. Heidelberg: Springer; 2013.
- [26] Eringen AC. Theory of micropolar elasticity. In: Liebowitz H, editor. *Fracture*. New York: Academic Press; 1968, p. 621–729.
- [27] Maugin GA. A historical perspective of generalized continuum mechanics. In: Altenbach H, Erofeev VI, Maugin GA, editors. *Mechanics of generalized continua: From the micromechanical basics to engineering applications*. Berlin: Springer; 2011.
- [28] Serpilli M. On modeling interfaces in linear micropolar composites. *Math Mech Solids* 2017;24(4):667–85.
- [29] Serpilli M, Rizzoni R, Lebon F, Raffa ML, Rodriguez-Ramos R. A size-dependent imperfect interface model for adhesively bonded joints considering strain gradient elasticity. *Int J Solids Struct* 2024;291:112720.
- [30] Brito-Santana H, de Medeiros R, Ferreira AJM, Rodríguez-Ramos R, Tita V. Effective elastic properties of layered composites considering non-uniform imperfect adhesion. *Appl Math Model* 2018;59:183–204.
- [31] Brito-Santana H, Christoff BG, Mendes Ferreira AJ, Lebon F, Rodríguez-Ramos R, Tita V. Delamination influence on elastic properties of laminated composites. *Acta Mech* 2019;230:821–37.
- [32] Fergoug M, Parret-Fréaud A, Feld N, Marchand B, Forest S. A general boundary layer corrector for the asymptotic homogenization of elastic linear composite structures. *Compos Struct* 2022;285:115091.
- [33] Huang Z-M. Mechanics theories for anisotropic or composite materials. *Adv Appl Mech* 2023;56:1–137, Editor(s): Stéphane P.A. Bordas.
- [34] Zhou J, Huang Z-M. Failures of laminates under nonpenetrative impacts. *Compos Struct* 2024;339:118096.
- [35] Backus GE. Long-wave elastic anisotropy produced by horizontal layering. *J Geophys Res* 1962;67(11):4427–40.
- [36] Abreu R, Durand S. Understanding micropolar theory in the earth sciences I: The eigenfrequency ω_p . *Pure Appl Geophys* 2022;179:915–32.
- [37] Hou M, Liu J, Soh AK. Modeling lattice metamaterials with deformable joints as an elastic micropolar continuum. *AIP Adv* 2022;12:065116.
- [38] Rukhlenko ID, Premaratne M, Agrawal GP. Theory of negative refraction in periodic stratified metamaterials. *Opt Express* 2010;18(26):27916–29.
- [39] Rodríguez-Ramos R, Yanes V, Espinosa-Almeyda Y, Otero JA, Sabina FJ, Sánchez-Valdés CF, Lebon F. Micro-macro asymptotic approach applied to heterogeneous elastic micropolar media. Analysis of some examples. *Int J Solids Struct* 2022;239–240:111444.
- [40] Rodríguez-Ramos R, Yanes V, Espinosa-Almeyda Y, Sánchez-Valdés CF, Otero JA, Lebon F, Rizzoni R, Serpilli M, Dumont S, Sabina FJ. Effective engineering constants for micropolar composites with imperfect contact conditions. In: Altenbach H, Bruno G, Eremeyev VA, Gutkin MY, Müller WH, editors. *Mechanics of heterogeneous materials*. Adv. struct. mater., vol. 195, Cham: Springer; 2023.
- [41] Yanes V, Espinosa-Almeyda Y, Rodríguez-Ramos R, Sánchez-Valdés CF, Sabina FJ, Montans FJ. Effective properties of centro-symmetric micropolar composites with non-uniform imperfect contact conditions. *Eur J Mech A- Solids* 2023;101:105038.
- [42] Kolpakov AG, Rakin SI. Chapter 18 - Comparative analysis of local stresses in unidirectional and cross-reinforced composites. In: Andrianov I, Gluzman S, Mityushev V, editors. *Mechanics and physics of structured media*. Academic Press; 2022, p. 395–416.
- [43] Benveniste Y, Miloh T. Imperfect soft and stiff interfaces in two-dimensional elasticity. *Mech Mater* 2001;33(6):309–23.
- [44] Hashin Z. Thin interphase/imperfect interface in elasticity with application to coated fiber composites. *J Mech Phys Solids* 2002;50(12):2509–37.
- [45] Penta R, Gerisch A. An introduction to asymptotic homogenization. In: Gerisch A, Penta R, Lang J, editors. *Multiscale models in mechano and tumor biology*. Lect. notes comput. sci. eng., vol. 122, Cham: Springer; 2017.
- [46] Glüge R, Kalisch J. The effective stiffness and stress concentrations of a multi-layer laminate. *Compos Struct* 2014;111:580–6.
- [47] Hassanpour S, Heppler GR. Micropolar elasticity theory: a survey of linear isotropic equations, representative notations, and experimental investigations. *Math Mech Solids* 2017;22:224–42.
- [48] Serpilli M, Rizzoni R, Lebon F, Dumont S. An asymptotic derivation of a general imperfect interface law for linear multiphysics composites. *Int J Solids Struct* 2019;180–181:97–107.
- [49] Benveniste Y. On the effect of debonding on the overall behavior of composite materials. *Mech Mater* 1984;3:349–58.
- [50] Kanit T, Forest S, Galliet I, Mounoury V, Jeulin D. Determination of the size of the representative volume element for random composites: statistical and numerical approach. *Int J Solids Struct* 2003;40(13–14):3647–79.